

3. SINGLE SEGMENT NANORODS

3.1. Introduction

As with the formation of the block copolymer templates, the synthesis of segmented nanorods with properties suitable for their use in cross-phase template assisted alignment is critical to this investigation. While work on the formation of the block copolymer templates focussed on the acquisition of rather “large” nanostructures (compared to that which is commonly used in the literature), the synthesis of free segmented nanorods is aimed towards the formation of comparatively small nanostructures at the lower limits of what has been achieved in the literature for single segment nanorods (<100nm diameter and <1 μm long), while maintaining control over segment size (both between synthesis batches and within) and composition in an effort to facilitate structural templating through the selective sequestration of these nanorods into the block copolymer microphases. Given that few methods have been developed in the literature with regards to the controlled synthesis and collection of such small nanorods (which typically becomes more difficult as the targeted nanorod size decreases), initial work on the formation of these nanoparticles is carried out on single segment nanorods, so that the conditions required for the formation and collection of small segmented nanorods with well controlled segment size and composition may be established. Before carrying out these experiments however, it is important to first decide upon a number of key parameters regarding the nanoparticle properties, and the conditions that are to be used initially in the synthesis and collection of the nanorods. One of the most important of these decisions is the selection of an appropriate synthesis template.

Template Selection

In order to obtain free nanorods, with dimensions suitable for their sequestration in the available microphase templates, one must select an appropriate synthesis template with the smallest pores possible for nanorod preparation. An initial comparison of the two most commonly used removable templates with sufficiently small pores; porous anodic alumina and track etched polycarbonate, suggests that porous anodic alumina is the more suitable template for acquiring small, free nanorods by electrodeposition, owing to the higher pore density (greater nanorod yields per template and better control over length resulting from the larger deposition area over which charge is passed), generally higher chemical and thermal resistance (allows use with many different plating solutions and conductive coating deposition methods) in addition to the easy removal of the template material to release the free nanorods (dissolves completely at high pH). Given that the apparatus required for custom synthesis of such templates is unavailable, commercially available porous anodic alumina with the smallest rated pore diameters (used principally as a filtration membrane) is examined for use (Whatman Anodisc, 20nm pores).

Scanning electron microscopy (SEM) images of the filtration surface (branched ends of the pores) of these membranes (fig 3.1) confirms the small rated pore diameter and high pore density, although the pore shape appears somewhat irregular. The pore structure of these membranes was also examined by SEM of their cross-sections. These small rated pore diameter membranes are reported to have an asymmetric pore structure, with 200nm diameter parallel pores extending throughout the bulk of the membrane, which then branch off to form the 20nm nominal diameter pores at the filtration surface. This pore structure is commonly used in commercial anodic alumina filtration membranes to facilitate fluid flow during filtration and to provide mechanical stability while allowing filtration at the rated level. SEM images of the membrane cross-section (fig 3.2) show that these branched pores only extend a short way into the membrane (<130nm) before becoming interconnected with adjacent pores. Given the restriction that

this place's on the nanorod lengths that may be made (after deposition of the sacrificial metal into the pores) without plating into the interconnected pore volume, such commercial membranes were deemed to be unsuitable for use as nanorod synthesis templates in this work.

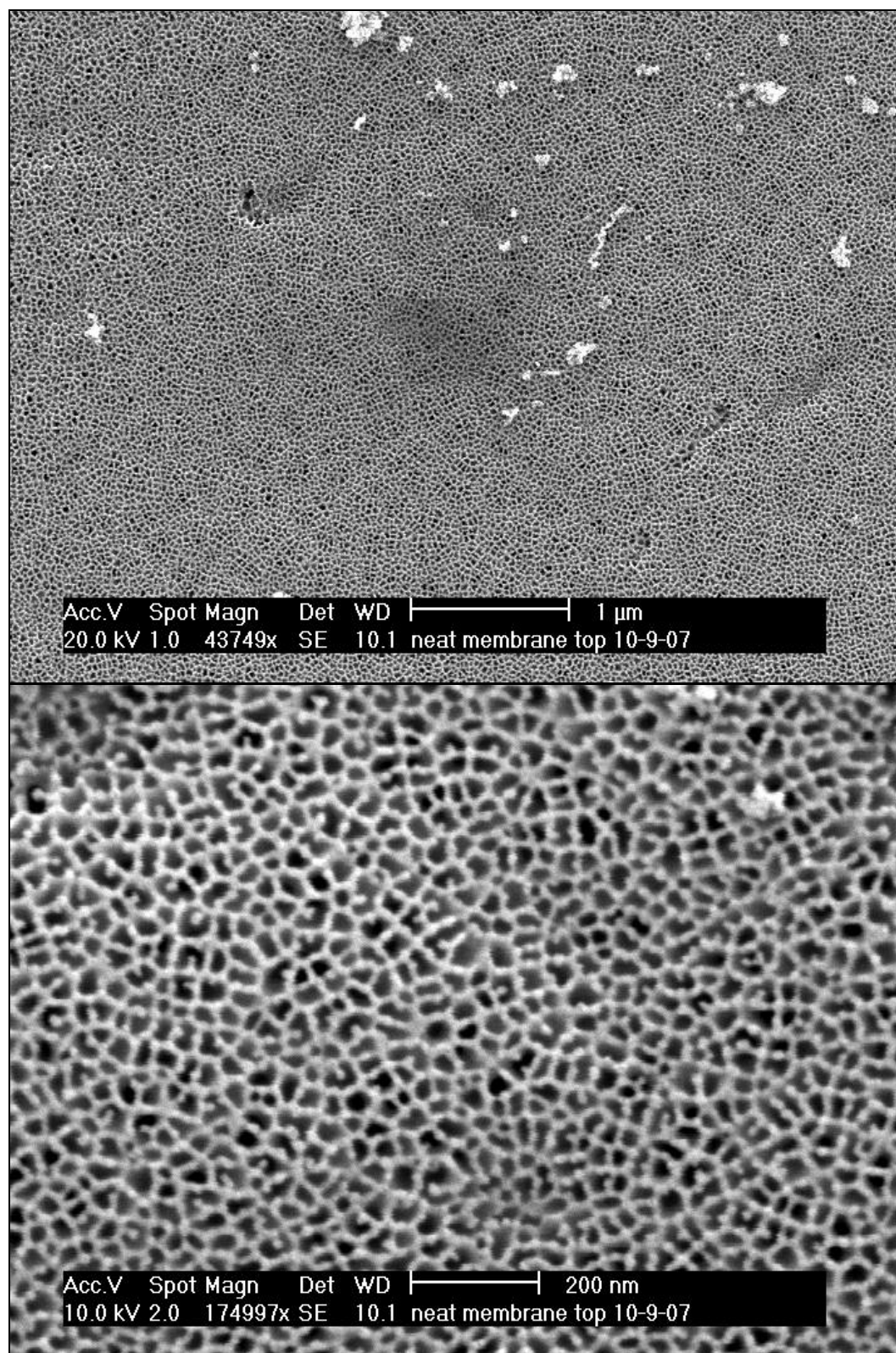


Fig 3.1: SEM images of the filtration surface of a commercially available porous anodic alumina filtration membrane (nominal 10nm pore diameter).

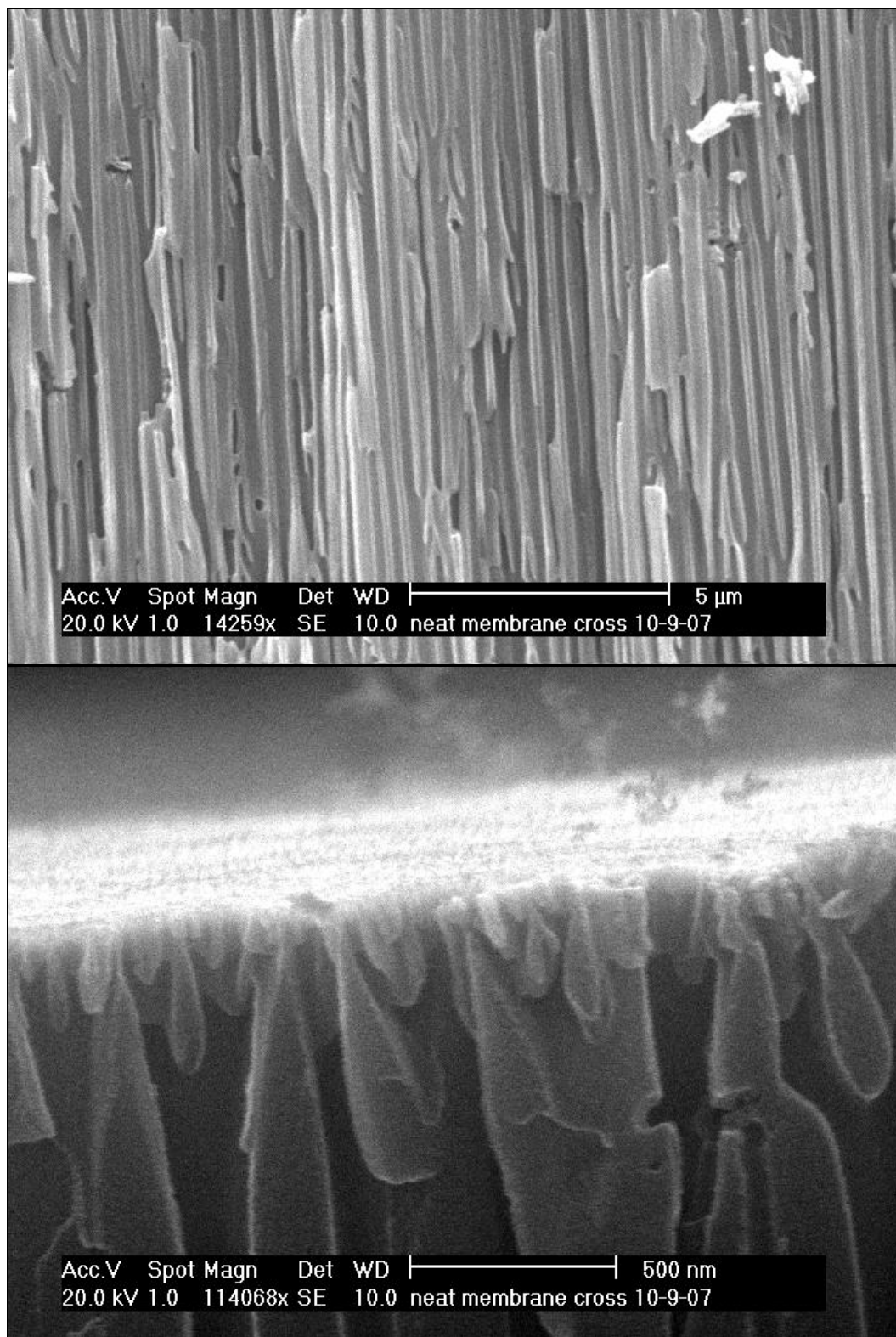


Fig 3.2: SEM images of the cross-section of a commercially available porous anodic alumina membrane (nominal 10nm pore diameter) showing the (top) pore structure in the bulk of the membrane and (bottom) the asymmetric pore structure at the branched (filtration) surface.

Commercially available track etched, polyvinylpyrrolidone coated polycarbonate membranes with the smallest available rated pore diameters (Sterlitech, 10nm nominal) were then examined by SEM to determine if the pore structure of these membranes is suitable for nanorod synthesis. SEM images of the surface of these membranes (fig 3.3) confirms that the pore density is markedly lower than that of porous anodic alumina, and shows that the surface pore diameters actually range between 10 - 30nm. Although determination of pore geometry directly by SEM images of membrane cross-sections is difficult to achieve (owing to sample damage that occurs during cross-sectioning of the membranes), the literature suggests that they have a largely non-intersecting [1], long straight “cigar” shaped geometry, (narrow entrances that bow outwards in the interior of the membrane) with a maximum diameter of ~40nm; a result of adsorption of species at the pore entrances protecting the substrate during chemical etching. [2-4] This form of pore geometry is commonly used in commercial track etched membranes in order to increase flow rates through these pores. Although the larger than rated pore sizes are not ideal, this form of template readily allows for the synthesis of individual, free-standing nanorods with acceptably small diameters (as block copolymers with the necessary microphase dimensions for nanorod sequestration can be synthesised), and so was selected for use in this work

Note that one important consideration when using this form of synthesis template is the method of template removal to yield the free nanorods. Although there is a well established procedure for the removal of polycarbonate membrane templates (dissolution in dichloromethane followed by centrifugation to collect the nanorods) [2, 5-7], this process needs to be repeated numerous times to completely remove the polymer. While for many applications the presence of residual amounts of dissolved polymer is not a problem, it is possible that the presence of this additional polymer may interfere with the microphase separation of the block copolymer template and the templating process when the nanorods are introduced. Therefore, thorough removal of the synthesis template material before inclusion of the nanoparticles into the block copolymer is desirable.

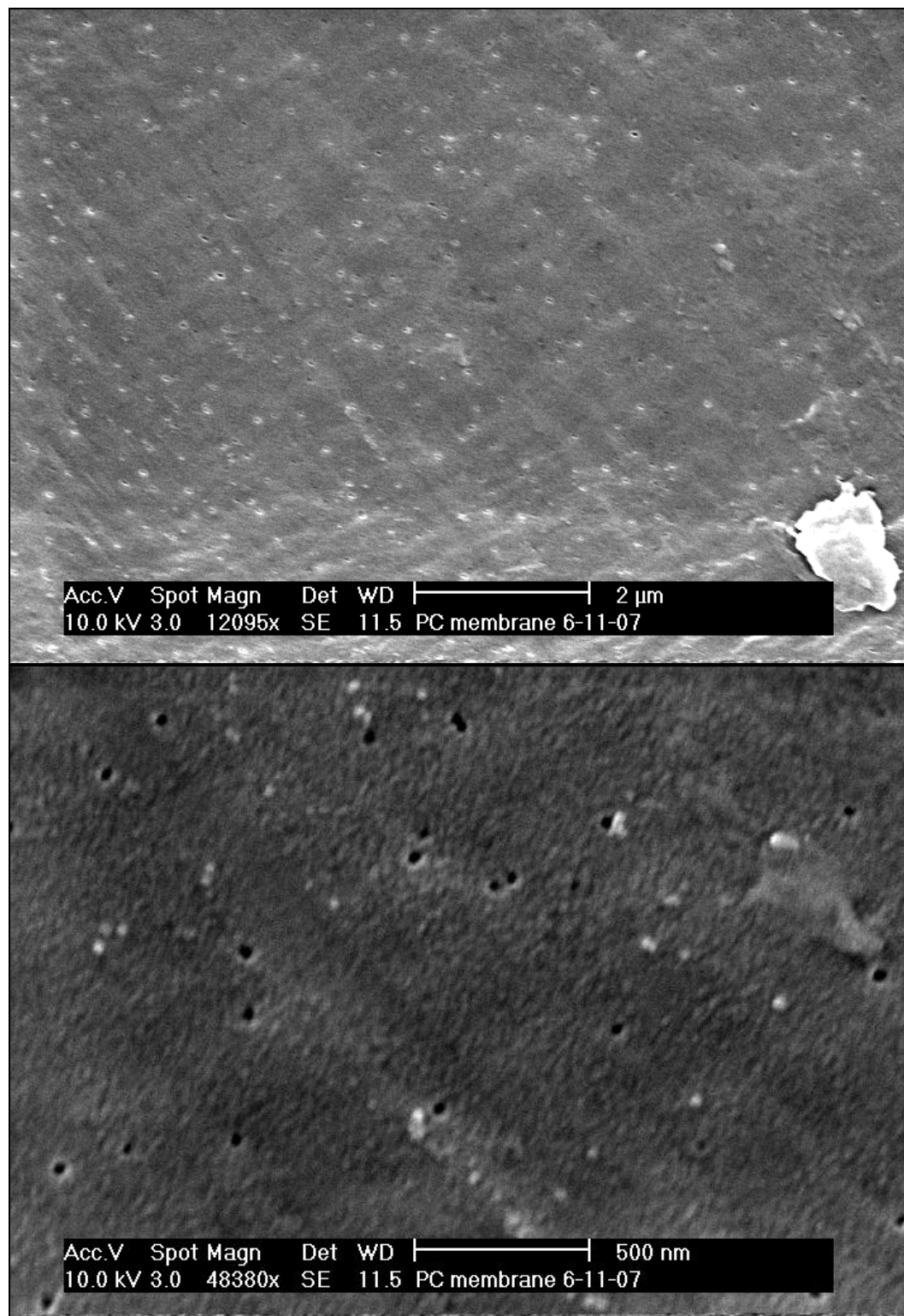


Fig 3.3: SEM images of the surface of a commercially available track etched polycarbonate membrane.

Conductive Coating

The selection of an appropriate conductive coating for one side of the membrane (to serve as a cathode in electrodeposition of metals into the pores), is important and a number of factors need to be taken into account. First, the coating should be such that deposition onto and removal from the synthesis template can occur without damaging the template or synthesised nanorods. Next, the structural integrity of the coating and the adhesion of the coating to the synthesis template are critical, as delamination of the coating prior to or during metal deposition will result in some of the metal being deposited outside of the confines of the pores. (fig 3.4) This in turn leads to reduced yields of nanorods (fig 3.4a) and a greater variation in nanorod length (fig 3.4b), with the concurrent variability in the relationship between nanorod length and passed charge (due to a cathode area that changes as deposition continues) also making it difficult to obtain nanorods with a set pre-determined length. For the same reasons, measures should be taken to ensure that the as coated conductive layer is devoid of cavities and pin-hole defects in order to completely seal this face of the membrane.

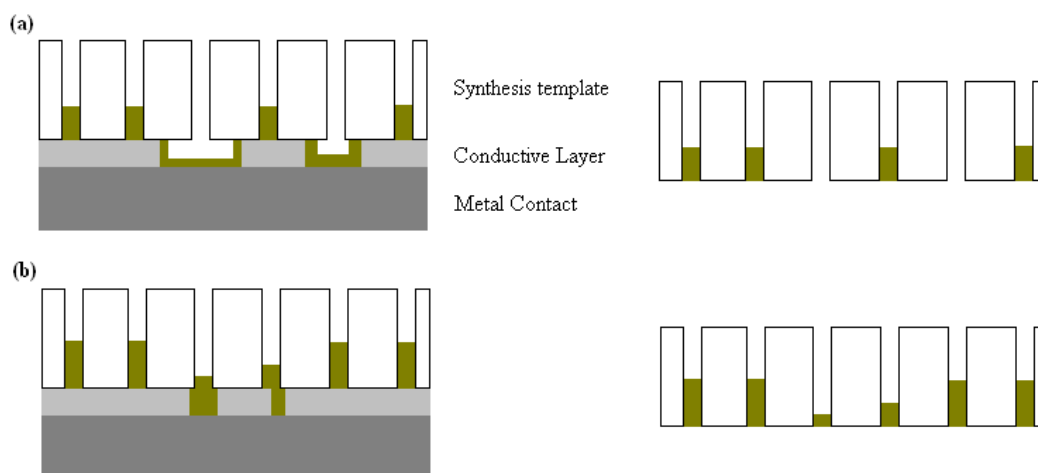


Fig 3.4: Porous membrane with a damaged/delaminated conductive backing exhibiting (a) a reduction in nanorod yields and (b) increased variation in nanorod length.

On the basis of these considerations, silver is chosen as the conductive layer material, as it is relatively cheap, highly conductive, may be deposited readily by sputter coating (a low temperature deposition process that will not damage the polycarbonate) and can be removed by chemical treatments (typically with nitric acid) that do not damage the template or most other metals that would be selected to form the segmented nanorods. A relatively thick layer (~200nm) of this metal is deposited to provide mechanical strength to this layer and to largely avoid pin-hole defects (fig 3.5). [2, 8-9]

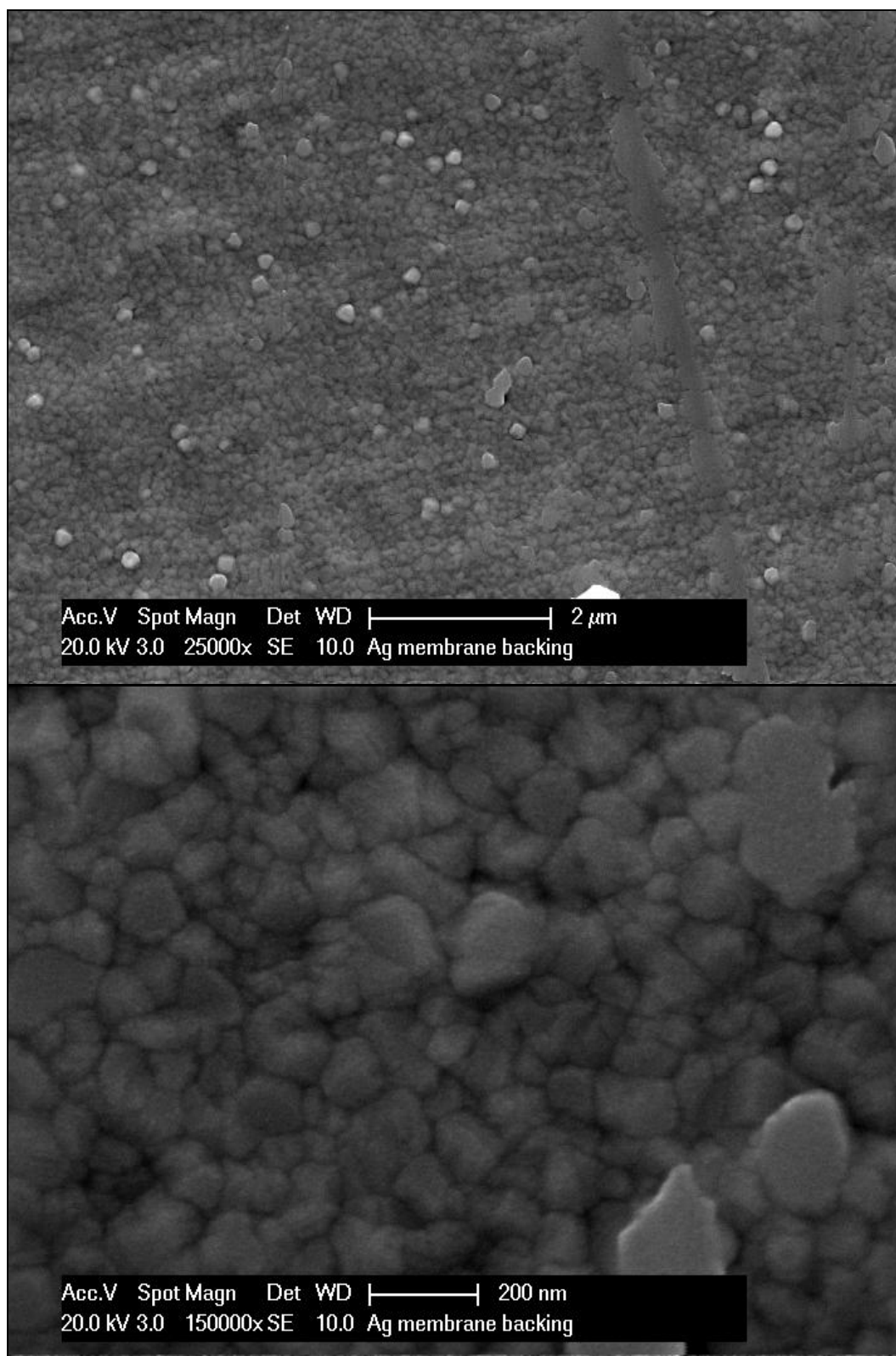


Fig 3.5: SEM of a 200nm thick Ag layer sputter coated onto a track etched polycarbonate membrane, which exhibits a largely pin-hole free surface.

To ensure that the coated side of all of the pores is completely sealed (so that subsequent deposition of metals to form the nanorods is entirely confined to the pores); a sacrificial layer of silver is electrodeposited into the pores (fig 3.6). [8, 10]

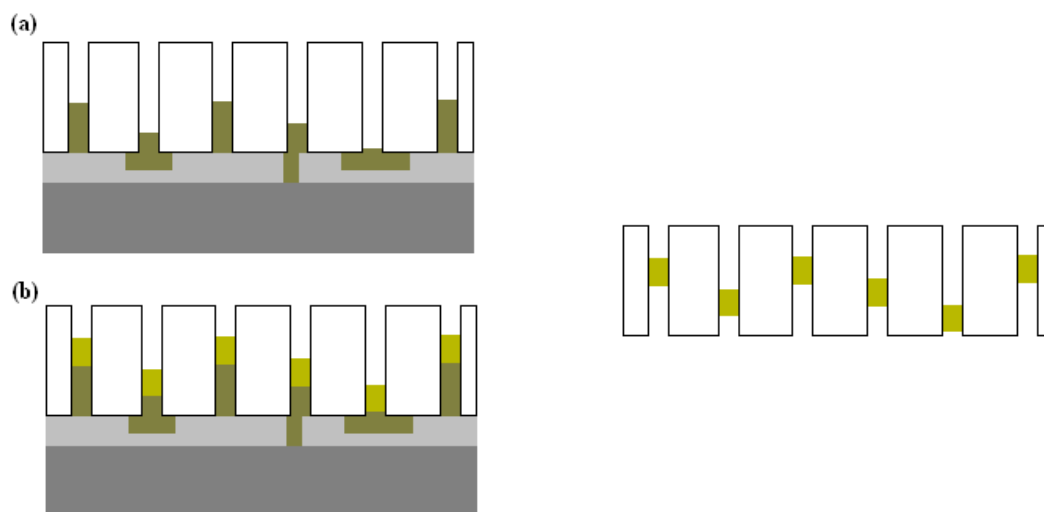


Fig 3.6: Porous membrane with a conductive coating containing voids and pin-hole defects that are (a) filled by electrodeposition of a sacrificial layer of metal followed by (b) deposition of the metal comprising the nanorods.

Silver is chosen as the electrodeposit materials for many of the same reasons that it is chosen to form the conductive layer. However, the vast majority of commonly available silver electroplating solutions are alkaline [11-13], meaning that these solutions will slowly attack the polycarbonate membrane. [6] The effect of a given silver plating solution upon the membrane (more specifically the membrane pore size) therefore should be evaluated before proceeding with the use of such a plating solution. The silver solution used in initial work is Ag_2O .

The deposition of a sacrificial layer of metal is also advantageous in that it serves to increase the adhesion of the conductive coating to the template by anchoring it to the template surface. The adhesion of the Ag conductive layer may be further increased by depositing a thin ($\sim 10\text{nm}$) under layer of chromium onto the polycarbonate template. This chromium layer is resistant to most treatments that

remove the Ag conductive layer, and so fragments of this layer will remain after template removal/nanorod collection. These fragments are advantageous in that they provide large flat surfaces to which the nanorods may adhere to, make location and imaging of large numbers of the nanorods by electron microscopy quicker and easier. However, the difficulty in removing this layer without damaging the template or metal nanorods contained within means that it cannot be used in work where the nanorods are to be collected and combined with the block copolymer, as it introduces an additional factor that may influence the block copolymer morphology and nanorod alignment.

Nanorod Composition

Clearly, the careful selection of the metals that are to comprise the individual nanorod segments is also important. In this work, only two metals need to be selected, as a diblock copolymer (two distinct microphases) is used as the template. Ideally, the selected metals will provide distinctly different surface chemistry (to enable selective functionalisation), not inter-diffuse appreciably under conditions of storage and use (reduces control over segment purity and lateral dimensions), be derived from electroplating solutions that do not react with the template material or previously deposited metal and are readily distinguishable by electron microscopy (particularly important in the later characterisation of multi-segment nanorods).

Nickel/Gold metal combinations satisfy these criteria. Both of these metals have been used extensively in the literature involving segmented nanorods that are selectively functionalised (Au with thiols and Ni/NiO with carboxylic acids), do not inter-diffuse appreciably (Ni is often used as a diffusion barrier material with Au) [14], can be readily distinguished by electron microscopy (owing to their very different electron densities) [9] and may be derived from a number of different electroplating solutions that are known to be compatible with polycarbonate membranes (the most commonly used solutions being gold cyanide and nickel sulfamate, both of which will be utilized in this work). [2, 5-7, 15-17]

One potential disadvantage of this metal combination is that the typical solution used to remove the Ag conductive layer, nitric acid, also attacks nickel metal. However, a concentrated nitric acid solution will also lead to extensive oxidation of the nickel, resulting in the formation of an oxide layer that prevents further acidic attack. [18]

Electrodeposition Conditions

The final aspect of the nanorod synthesis that needs to be considered is the electrodeposition conditions. In order to obtain high purity nanorod segments, sequential electrodeposition is employed using individual plating solutions with rinses between segment preparations (as opposed to the use of a single mixed metal solution with pulsed potential deposition). Critical to obtaining pure segments under these conditions (and a well controlled nanorod length vs. passed charge relationship) is the efficient removal of the residual metal species from the pores (left from previous depositions). The most common method used to remove such residual species is multiple rinses of the membrane with pure water; thus this method will be used initially in this work. However, given the small pore diameters and depth of the pores, such rinsing may not be adequate, and so alternative methods may also need to be examined. Potentiostatic (constant potential) deposition rather than galvanostatic (constant current) deposition is utilised in these nanorod syntheses, as galvanostatic deposition has been generally unsuitable for deposition into pores with diameters less than 35nm. [19]

Potentiostatic deposition also allows the plating process to be monitored through its current response. [20] Based on the literature involving the use of the selected solutions, a potential of -1.0 V (vs. an Ag/AgCl reference electrode) will be used for all metal depositions. [2, 6, 10, 20-22]

Summary

In summary, the work presented in this chapter concerns the synthesis and collection of single segment nanorods with dimensions at the lower limit of that which has been achieved in the literature; the principal focus of this work being on the elucidation of the synthesis conditions that result in the highest level of control over the nanorod segment length and composition, so that the conditions required for the preparation of multi-segmented nanorods with properties amenable for their use in cross-phase template directed alignment with microphase separated block copolymers may be determined.

The nanorods prepared in this work comprise individually of either gold or nickel and are prepared by sequential DC electrodeposition of these metals into the pores of commercially available polycarbonate filtration membranes. Initial studies are performed to characterise the synthesis of such nanorods under a set of standard conditions drawn from the literature. Based on these results, experiments are then performed to determine the synthesis conditions under which control over the nanorod dimensions and purity are highest. Finally, the effectiveness of common literature methods in collecting and isolating the nanorods from the synthesis template is evaluated and alternative methods investigated.

3.2. Experimental Methods and Materials

3.2.1. Membrane Preparation

Polycarbonate filter membranes (Sterlitech, 47mm diameter, 10nm nominal pore diameter), which serve as the nanorod synthesis template, are sputter-coated with metal to form a conductive layer using a Cressington 208HR sputter coater equipped with an MTM20 quartz crystal microbalance thickness controller (0.1nm resolution) at a current of 80mA in an argon atmosphere (0.04mbar).

In a typical preparation, the membrane is placed onto a glass plate and secured using metal stubs that are stuck to the glass (to prevent movement of the membrane during evacuation/backfill of the coating chamber). The secured membrane is then sputter-coated with a layer of chromium (10nm); with 1min long cool down periods after every 5 min of sputter-coating. This is performed to prevent significant temperature increases and thus damage to the membrane. The shutter (a shield between the sputter target and the membrane) is also left closed for the first 5 min period of this deposition in order to largely prevent the sputtering of chromium oxide (that forms on the surface of the sputter target during air exposure) onto the membrane. After ~ 5 min, the chromium oxide layer (purple plasma) is removed, after which sputtering of pure chromium (blue plasma) occurs. This chromium coating is followed by the deposition of a layer of silver (200nm), which is sputtered in 50nm thick steps with a 1 min cool down period between depositions (to prevent undue heating). The shutter is left closed for the first 10nm of silver deposition to allow for the formation of an adhesion layer.

Note that although attempts to minimise heating of the membrane ensures temperatures are not being reached that result in membrane damage, some degree of heating remains unavoidable. As a result of the different thermal expansion coefficients of the polymer and metal layers, the polycarbonate membranes

coated in this way tend to curl up into a tube with the metal coated side facing outwards upon cooling to room temperature.

3.2.2. Nanorod Synthesis

Plating Solutions

434 Neutral Soft Gold, High-Speed Nickel Sulfamate and Silver Cyless II solutions were purchased from Technic inc. as plating solutions used in nanorod synthesis. These plating solutions have well established electrochemistry, provide relatively pure metal deposits and have been used in the preparation of segmented nanorods in the literature. [6, 23-25]

Electrodeposition

In order to deposit metal selectively into the pores of the silver coated membrane, restricted access to the open ends of the pores by the plating solution is provided by the use of a glass cell as shown in fig 3.7.

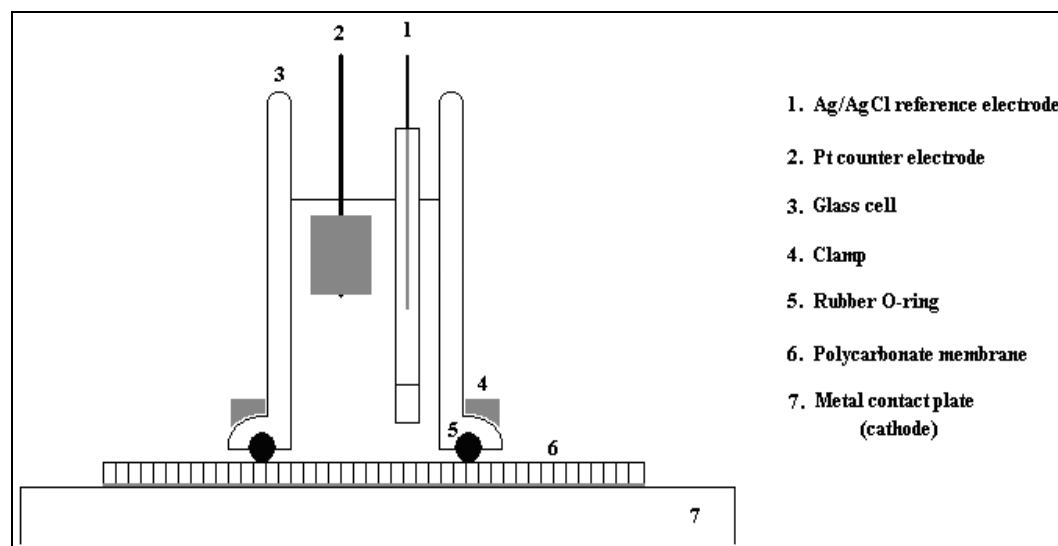


Fig 3.7: Setup of the electrodeposition apparatus.

This setup is assembled via the following steps:

- The Ag coated membrane is placed silver side down onto a steel contact plate, which then serves as a conductive contact between the silver coating and the source of the potential difference that is to be applied. Given that the membrane is curled up after sputter coating, the membrane needs to be unfurled onto the metal contact plate without damage. This is accomplished by placing 1-2 drops of distilled water onto the contact plate (near the edge) and positioning the curled up membrane on the water (as shown in fig 3.8). The hydrophilic silver coating, along with the water's surface tension, results in the membrane unfurling to lie flat on the metal contact plate.

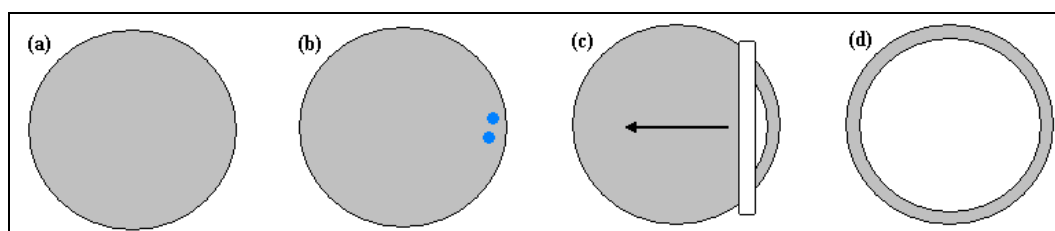


Fig 3.8: procedure for the unfurling of the Ag coated polycarbonate membrane onto (a) the metal contact plate which has (b) 1-2 drops of water deposited onto it near the edge. The curled up membrane is then placed onto these drops such that (d) the membrane may unfurl to cover the metal contact plate.

- The rubber O-ring (34mm diameter) is then carefully placed onto the membrane and the glass cell is placed onto the O-ring so that it fits into the ground glass groove. The glass cell is then secured with a clamp.

In a standard nanorod preparation, the following procedure is then performed to deposit metal into the pores to form nanorods.

- The glass cell is filled with millipore nanopure water (18 M Ω) and the membrane is soaked for 30 min. This is performed to ensure that the pores are

fully wetted prior to introduction of metal plating solutions so that deposition may commence in all pores simultaneously. [2, 23]

- Following this period, the glass cell is emptied of the water, and is then replaced with the silver plating solution in order to deposit a sacrificial silver layer at the base of the pores. A clean Platinum counter electrode (serving as an inert anode) with a surface area of $\sim 2\text{cm}^2$ (significantly greater than that of the cathode) and Ag/AgCl reference electrode are then suspended within the plating solution. Ideally, the reference electrode is placed several millimetres away from the membrane.
- The electrodes and metal contact plate are then connected (using alligator clips) to the corresponding terminals of a BAS 100b electrochemical analyser (which will serve as the potential difference source).
- A potential of -1.0V is applied to commence the electrodeposition.
- The current and passed charge (integral of current vs. time) is monitored over the course of the electrodeposition and after the desired amount of charge has passed (equivalent to a specific volume of metal), the potential is removed and the counter and reference electrodes are withdrawn from the solution and rinsed thoroughly with deionised water.
- The plating solution is then discarded and the glass cell and membrane is rinsed with nanopure water several times to remove residual silver solution. The cell is then filled with a metal plating solution corresponding to the metal that is to comprise the nanorod segment, and the above process repeated with the appropriate current limit (table 3.1).

Table 3.1: Current limits for the deposition of metals (given as current per unit electrode area). *

Metal plating solution	Limiting current density (mA/cm²)
High-Speed Nickel Sulfamate	43.1 – 430.6
Neutral Soft Gold	1.1 – 10.8

Nanorod Collection

To collect the nanorods, the membrane is first subjected to a brief (10 sec) treatment with 4M nitric acid in order to dissolve the sacrificial silver. The membrane is then rinsed with distilled water, blotted dry and placed into a 10ml polyethylene centrifuge tube. The tube is then filled with 6ml of dichloromethane and the membrane is dissolved with brief sonication and shaking. The nanorods are then collected into a pellet by centrifuging the suspension at 3200RPM (1090g) for 30 min. The supernatant is removed and replaced with 3ml of pure dichloromethane and the pellet is broken up with mild sonication. This process is repeated several times to remove the residual polycarbonate. This process is then further repeated twice more using ethanol instead of dichloromethane, with the final product being stored in 3ml of ethanol. [8, 10, 21, 23, 26]

3.2.3. Nanorod Characterisation

Nanorods are characterised through the use of electron microscopy, which is performed using the following procedures:

Transmission Electron Microscopy

For standard imaging, the nanorods (from one membrane) in 3ml of ethanol are sonicated briefly and one drop of the resulting suspension is deposited onto a Cu grid (200 mesh) that is coated with a formvar membrane. The ethanol is allowed

* Current density data provided by the plating solution supplier, Technic inc.

to dry, and the resulting sample is imaged using a Jeol 1200ex TEM equipped with a Megaview III camera at an accelerating voltage of 80kV and a spot size of 3.

If high resolution images are desired or elemental composition of sample features needs to be determined (using energy dispersive x-ray analysis or EDAX), imaging is performed using a Phillips CM200 TEM equipped with a Gatan 832 SC1000 CCD camera and EDAX at an accelerating voltage of 200kV. Spot size for general imaging is 3, but may be as small as spot size 7 for collecting EDAX data on specific areas of structures as small as the nanorods.

Scanning Electron Microscopy

Nanorods (from one membrane) in 3ml of ethanol are sonicated briefly and one drop of the resulting suspension is deposited onto the surface of carbon tape on a steel SEM stub. After the ethanol has dried, the sample on the stub is imaged using a Phillips XL30 FEGSEM equipped with EDAX and a backscattered electron detector at an accelerating voltage of 10kV, a spot size of 3 and a working distance of ~10mm.

3.2.4. Other Sample Characterisation

Other samples examined in the work presented in this chapter by SEM are prepared in a similar manner as used for the nanorod samples.

In the case of solid samples, the material is secured to a steel SEM stub through use of adhesive carbon tape. In the case of electrically insulating samples, the sample is sputter coated with a thin (3nm) layer of platinum to enhance the image resolution, which is typically reduced when the sample accumulates charge from the electron beam.

3.3. Results and Discussion

3.3.1. Initial Experiments

Initial experiments are performed to characterise the nanorods synthesised under a set of “standard” conditions that are drawn from the literature. The first such experiment that is carried out is an examination of the effect of the selected silver solution (which has been used in the literature) upon the polycarbonate membrane, as such high pH solutions have been noted to chemically attack polycarbonate. This may influence the pore size and geometry and therefore, the dimensions of the nanorods produced from subsequent electrodeposition. This study is then followed by the characterisation of trial electrodepositions of gold and nickel into the membranes to form nanorods, using the deposition conditions outlined in section 3.2.2.

Effect of the Silver plating solution on the Polycarbonate synthesis template

The effect of the silver plating solution upon the polycarbonate templates is evaluated by collecting SEM images of the membrane surfaces that have been soaked in nanopure water for a period of 30 minutes before being exposed to the silver plating solution for a period of 3 minutes (the approximate typical silver deposition time to provide a small sacrificial silver layer) to emulate the conditions under which the silver plating solution will be used.

At low magnification, there exists clear evidence of chemical attack upon the polycarbonate, with a marked increase in surface roughness (fig 3.9).

Examination of the diameter of the pore entrances at higher magnifications (fig 3.10) shows that there is an increase in pore entrance diameter, which has been determined to span the range 20 – 46nm (up from 10 – 30nm prior to exposure to the silver plating solution). Although this increase in pore entrance diameter is significant, the degree of chemical attack by the silver solution over this short

period of time *within the depth* of the pores (where the deposition of metal comprising the nanorods will occur due to the use of a sacrificial layer of silver) is unknown, and cannot be determined directly due to difficulties in obtaining images of the membrane cross-section (as discussed in the introduction). In order to resolve whether the nanorods produced using the silver solution that forms the sacrificial layer will have diameters that are still small enough for acceptable use in template assisted alignment with the available block copolymers, this silver solution will be used in the initial trial electrodeposition experiments, and the diameter of the resulting nanorods will then be examined.

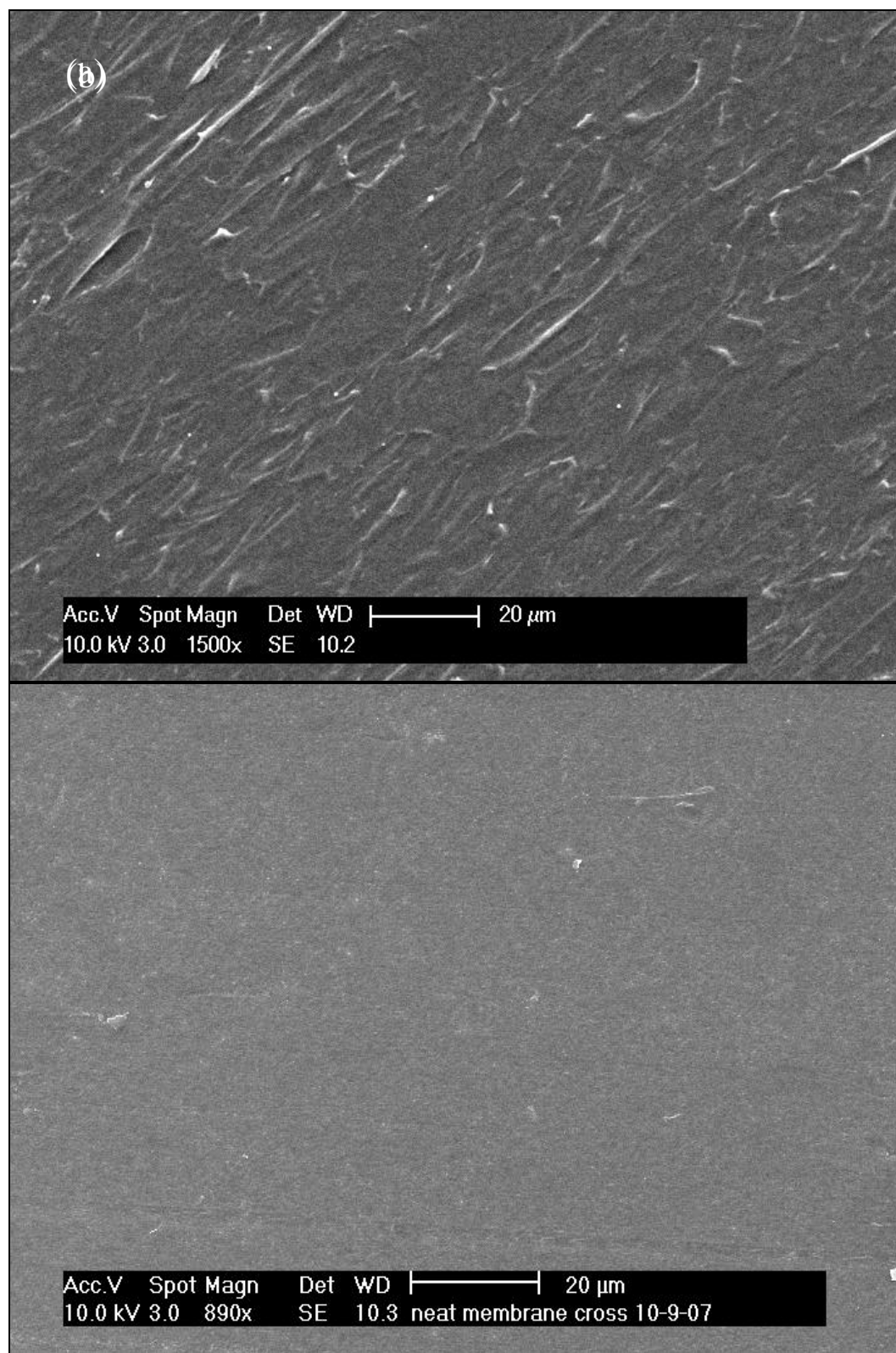


Fig 3.9: SEM images of (a) Ag treated polycarbonate and (b) untreated polycarbonate membrane.

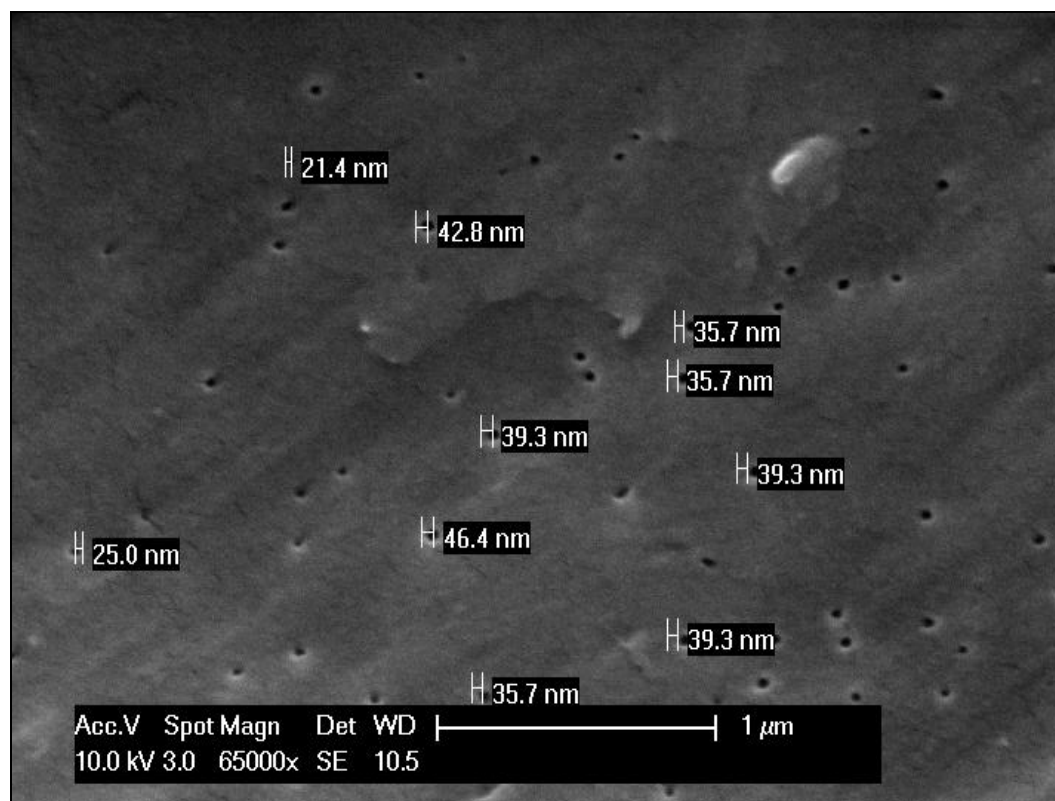


Fig 3.10: SEM image of Ag treated polycarbonate at high magnification.

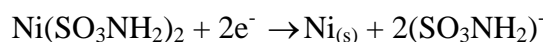
Trial electrodeposition: Nickel

Before performing the trial electrodepositions, it is helpful to first calculate an estimate for the amount of charge that should be passed in order for a given volume of metal to be deposited, and to therefore acquire a specific nanorod length. Assuming a current efficiency of 100%, the amount of metal deposited for a given amount of passed charge may be determined using Faraday's law:

$$Q = m \cdot n \cdot N_a \cdot Q_e$$

where Q is the total charge passed (coulombs), m is the number of moles of metal reduced, n is the number of electrons involved in the reduction reaction, N_a is Avogadro's constant and Q_e is the charge of an electron (coulombs). In the case

of the deposition of nickel from a nickel sulfamate solution, 2 electrons are involved in the reduction of a single nickel atom.



Therefore, the charge required to deposit 1 mole of nickel atoms from the nickel sulfamate plating solution is 192970.68 C.

Now, assuming an average pore diameter of 40nm (in the depth of the pores where nickel deposition will take place), a nanorod segment of 100nm has a volume of:

$$\pi \cdot (2 \cdot 10^{-6})^2 \cdot 10^{-5} = 1.2566 \cdot 10^{-16} \text{ cm}^3$$

From the density and molar mass of nickel metal, the number of moles of nickel atoms in this 100nm long nanorod segment is therefore:

$$\frac{(1.2566 \cdot 10^{-16} \text{ cm}^3) \cdot (8.912 \text{ g / cm}^3)}{58.71 \text{ g / mol}} = 1.9075 \cdot 10^{-17} \text{ mol}$$

The total number of moles of nickel deposited into the membrane to obtain 100nm long segments (assuming a uniform deposition) depends upon the number of pores into which the metal is deposited. From SEM images of the surface of the selected polycarbonate membranes, a pore density of 5.3125 pores/ μm^2 of membrane area is determined. The membrane area exposed to the plating solutions in a typical deposition is equal to the area enclosed by the rubber O-ring used to ensure that the plating solution is only exposed to the open side of the pores (as described in section 3.2.2). In this work, the membrane area exposed to a given metal plating solution is:

$$\pi r^2 = \pi(1.7 \cdot 10^4)^2 \mu\text{m}^2 = 9.079 \cdot 10^8 \mu\text{m}^2$$

resulting in metal deposition into a total of $4.823 \cdot 10^9$ pores per membrane. Thus, a total of $9.2 \cdot 10^{-8}$ moles of nickel atoms are deposited into the membrane to obtain 100nm long segments. This requires a passed charge of $1.7753 \cdot 10^{-2}$ C.

Based on this estimate, nanorod samples are prepared by passing a charge of 0.25C (a higher than calculated charge is used to compensate for assumptions such as 100% current efficiency and pore diameter before exposure to the Ag plating solution). TEM images of the resulting nanoparticles are shown in fig 3.11. From these images, it is apparent that metal deposition is carried out successfully, resulting in the formation of rod shaped nanoparticles with a wide range of lengths (on the order of 500nm) and diameters ranging from 30 – 50nm. EDAX analysis of these nanoparticles (fig 3.12) confirms that they consist almost entirely of nickel metal (the copper signal being assigned to the presence of the TEM grid). High resolution TEM images of the nickel nanorods (fig 3.13) indicate that they possess a polycrystalline structure.

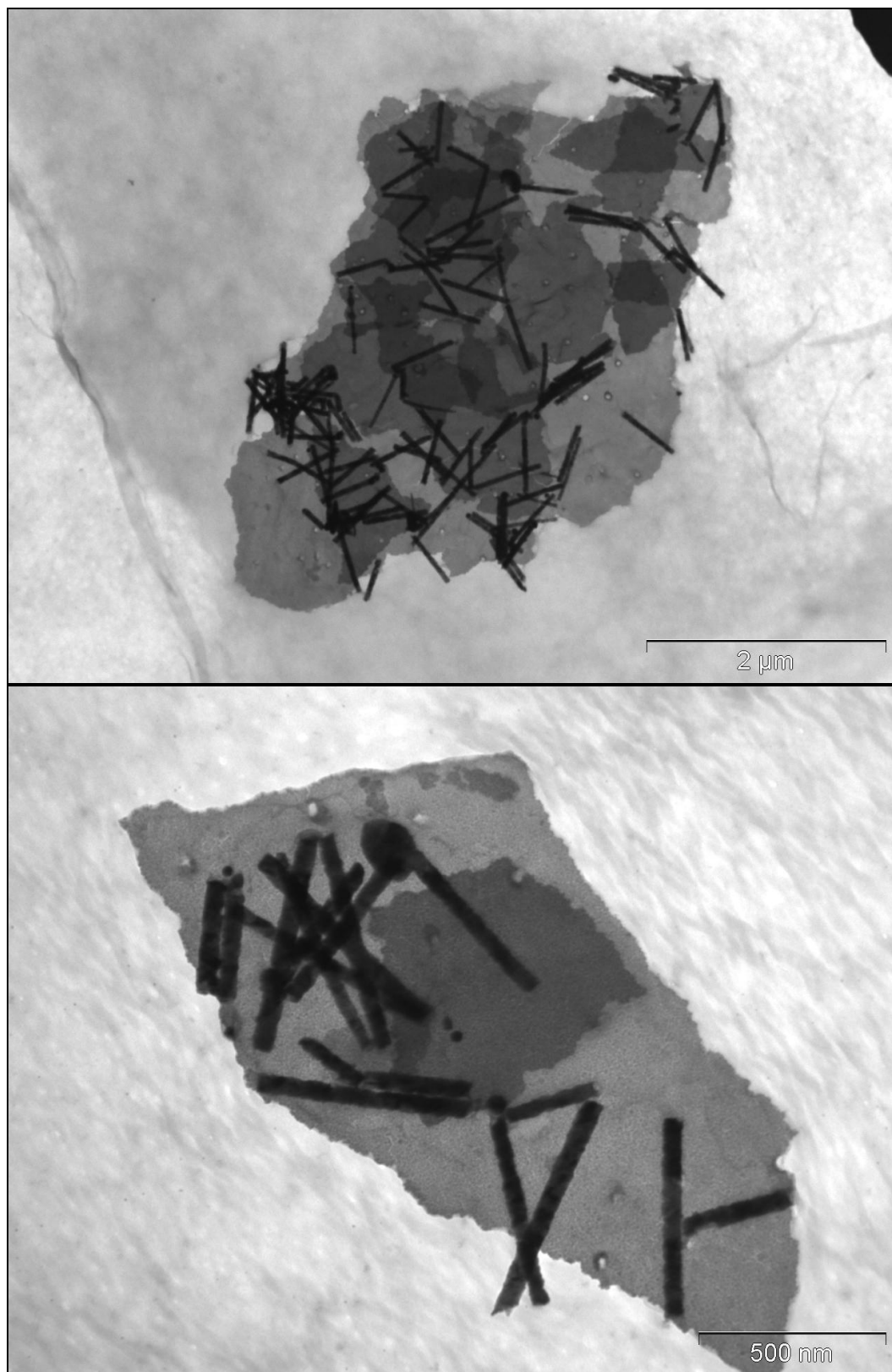


Fig 3.11: TEM images of Ni nanorods synthesized under literature derived conditions.

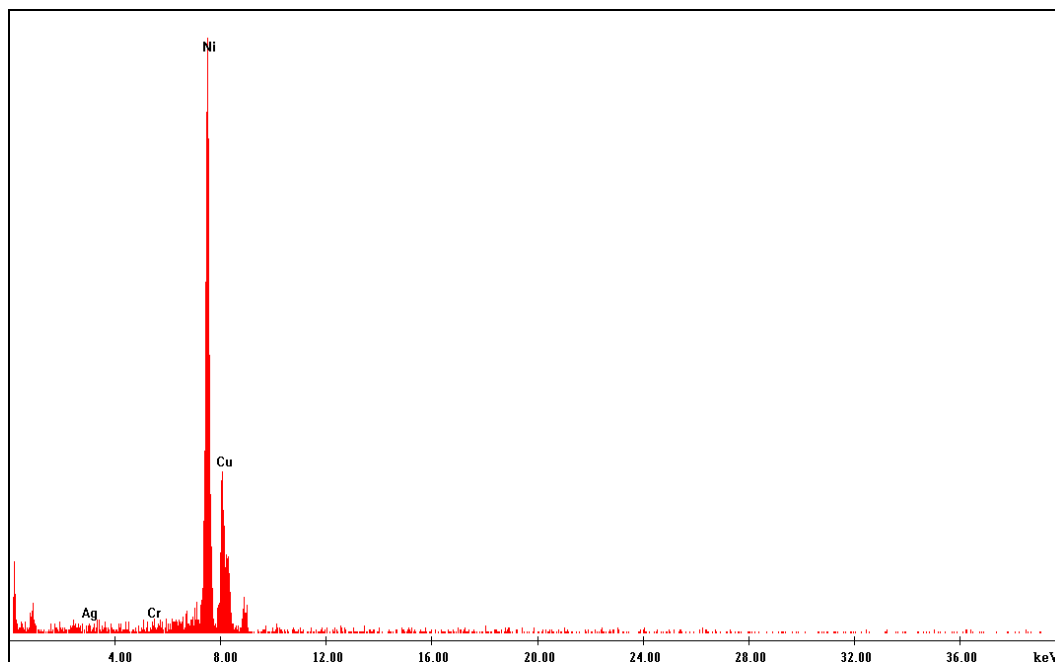


Fig 3.12: EDAX spectrum of Ni nanorods.

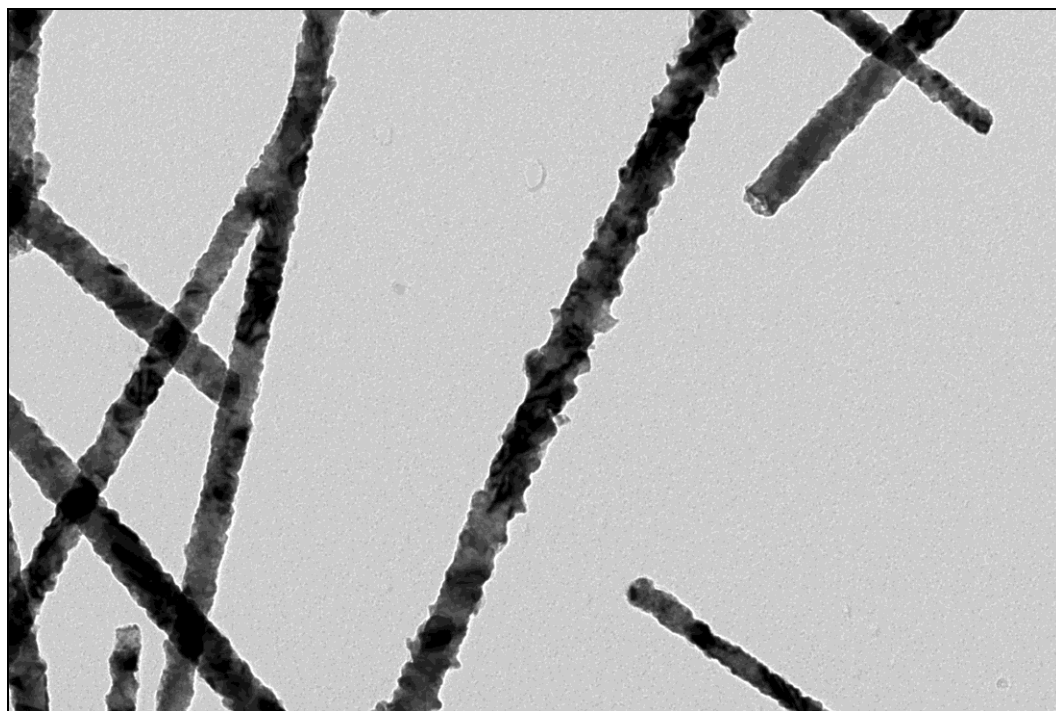


Fig 3.13: High resolution TEM image of nickel nanorods synthesized under literature derived conditions.

These TEM images also prominently feature thin, perforated plates of irregularly shaped material, to which the majority of the nanorods in the sample appear to

adhere (fig 3.14). These plates are most likely to be fragments of the chromium adhesion layer that is sputter coated onto the polycarbonate membranes prior to silver coating, based on the presence of circular holes in these plates with diameters and occurrence similar to that of the pores of the polycarbonate membrane and EDAX analysis (fig 3.15), which indicates that these plates are comprised of chromium.

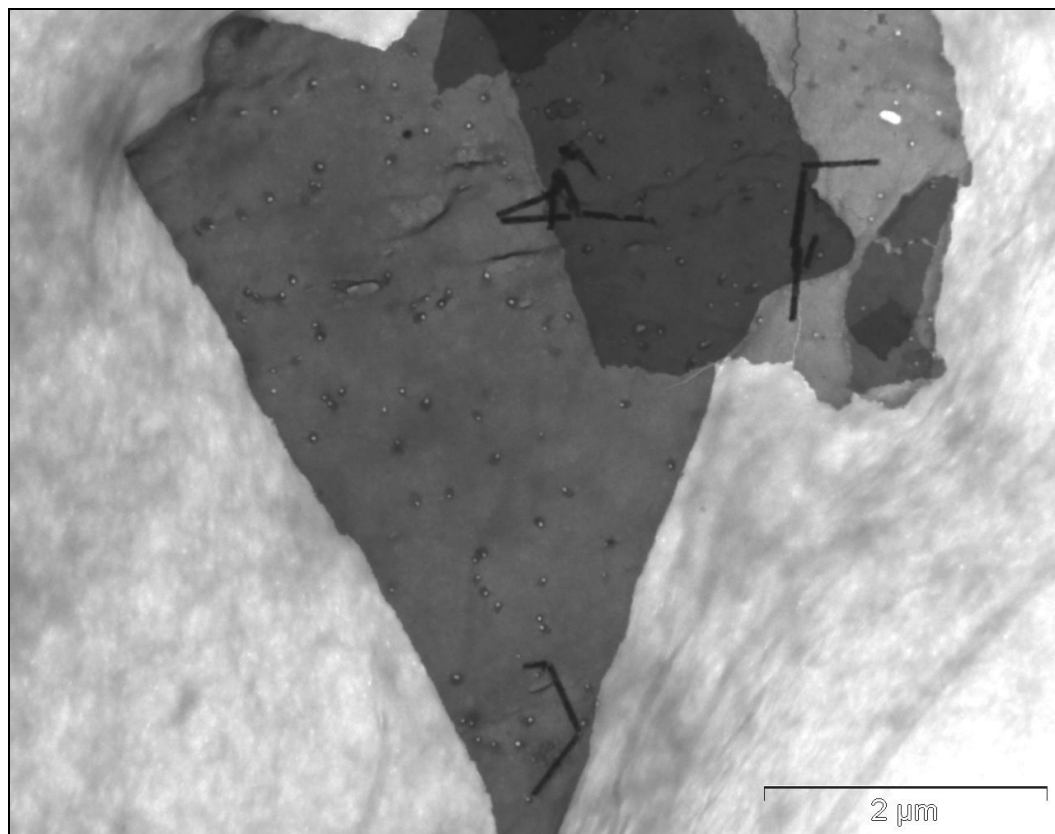


Fig 3.14: TEM image featuring the perforate, plate like fragments of material observed in the nickel nanorod samples.

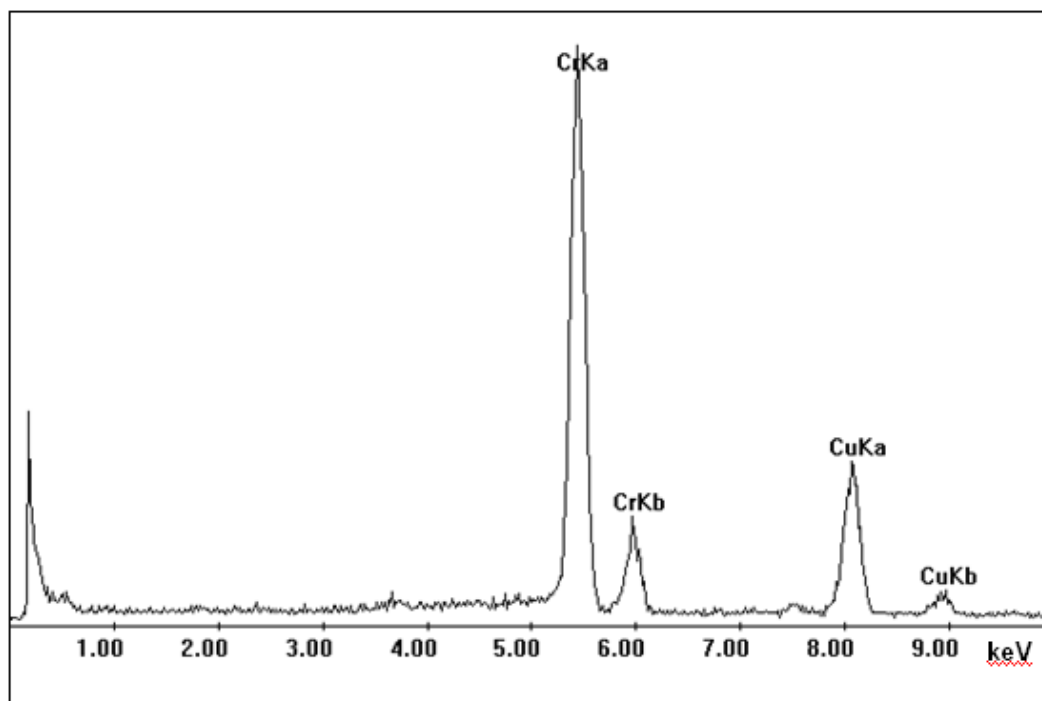


Fig 3.15: EDAX of the perforated, plate like fragments of material in TEM images of nickel nanorods.

The deposition process yielding these nanorods is characterised by the current vs. time data for this electrodeposition, which shows that the deposition proceeded with an initially high current that rapidly decreases to a steady value of $\sim 4.2\text{mA}$ (fig 3.16).

This deposition behaviour may be explained by considering two effects. The high initial spike in current is ascribed to charging of the cathode electric double layer upon application of the non-equilibrium potential difference between the anode and cathode, as the increase in potential difference leads to an increase in the charge separation in the diffuse double layer; the movement of these charges being experienced as a current. [27-28] The subsequent gradual decrease in current towards a steady value is indicative of the formation of a diffusion layer within the pores, due to the rate of reduction of metal species at this overpotential being greater than the rate of replenishment of the metal species near the cathode by mass transport into the pores from the bulk solution. This suggests that the deposition process is mass transport controlled. [27]

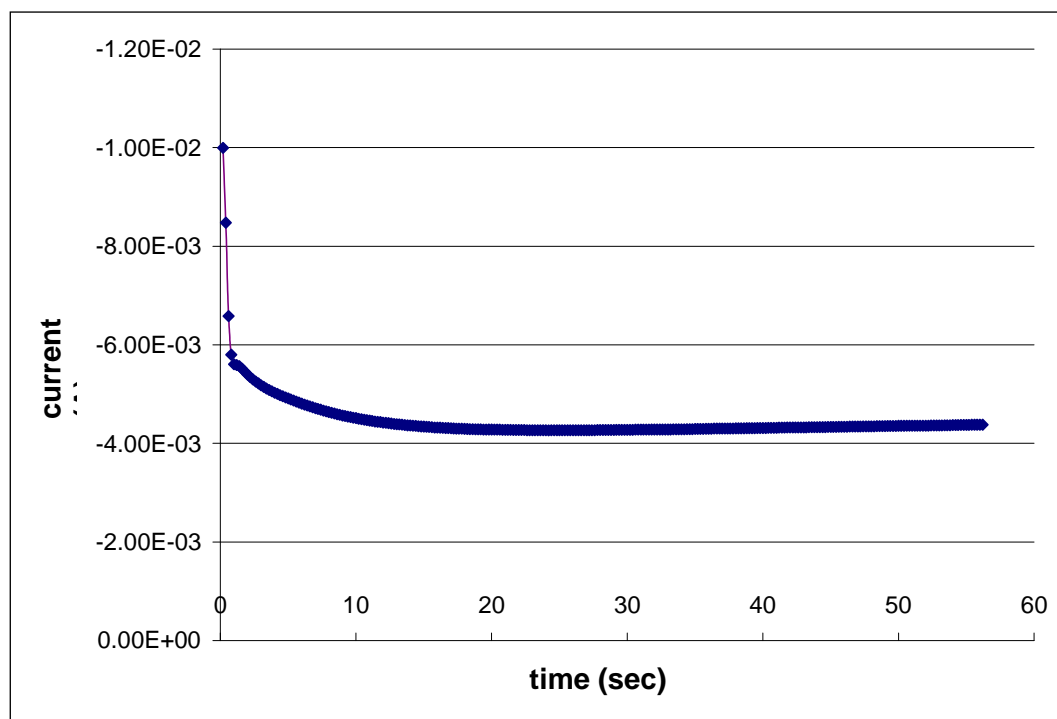


Fig 3.16: A typical current vs. time data for the electrodeposition of nickel from a nickel sulfamate plating solution into the pores of a polycarbonate filtration membrane.

The resulting current density for this mass transport limited deposition is determined by first calculating the total cathode area within the pores. Knowing that the pore diameter varies between 30 - 50nm at the depth in the pores where the metal deposition takes place (based on TEM images of the nanorods), the cathode area per pore (A) is calculated to be: †

Pore diameter (D): $30\text{nm} < D < 50\text{nm}$

Pore density: 6×10^8 pores / cm^2

Exposed membrane area: 9.08 cm^2

† Note that the cathode surface area may be slightly larger than the calculated values due to surface roughness of the metal deposits.

Therefore, the total cathode area (\tilde{A}) lies in the range:

$$0.0385\text{cm}^2 < \tilde{A} < 0.107\text{cm}^2$$

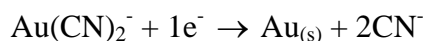
yielding a current density (I_d) of:

$$39.25\text{mA/cm}^2 < I_d < 109.09\text{mA/cm}^2$$

which is largely within the optimal range of current densities for this plating solution (43.1 – 430.6 mA/cm²).

Trial electrodeposition: Gold

As with the nickel deposition, it is helpful to first estimate the amount of charge required to deposit a given volume of gold before carrying out the trial electrodeposition experiment. As before, the charge required for the formation of a gold segment of a given length may be estimated using Faraday's law. In the case of gold deposition from a gold cyanide plating solution, one electron is required for the reduction of a single gold atom.



Therefore, in this work, a charge of 96485.34 C is required to reduce one mole of gold atoms. Knowing the number (and dimensions) of pores in the membrane template within which deposition of metal occurs, as well as the density and molar mass of gold, the amount of gold that needs to be reduced to form 100 nm long nanorod segments (assuming uniform metal deposition) is estimated at $5.9384 \cdot 10^{-8}$ moles. Consequently, a charge of $5.73 \cdot 10^{-3}$ C needs to be passed to form nanorods of this length.

Based on this estimate, a charge of 0.05 C is passed for this gold electrodeposition experiment (higher than the calculated estimate due to the assumptions that are made in its determination as discussed earlier). Current vs. time data for this electrodeposition (fig 3.17) exhibits the same characteristics as that of the deposition of nickel, indicating that this deposition is also a mass transport controlled process. Notably, the steady state current for the gold electrodeposition is significantly smaller than that for the nickel deposition ($\sim 0.35\text{mA}$). This is ascribed to the more restricted mass transport of the negatively charged gold species into the pores compared to that of the neutral nickel species, owing to the contribution of ion migration (anions migrate away from the cathode in an electric field).

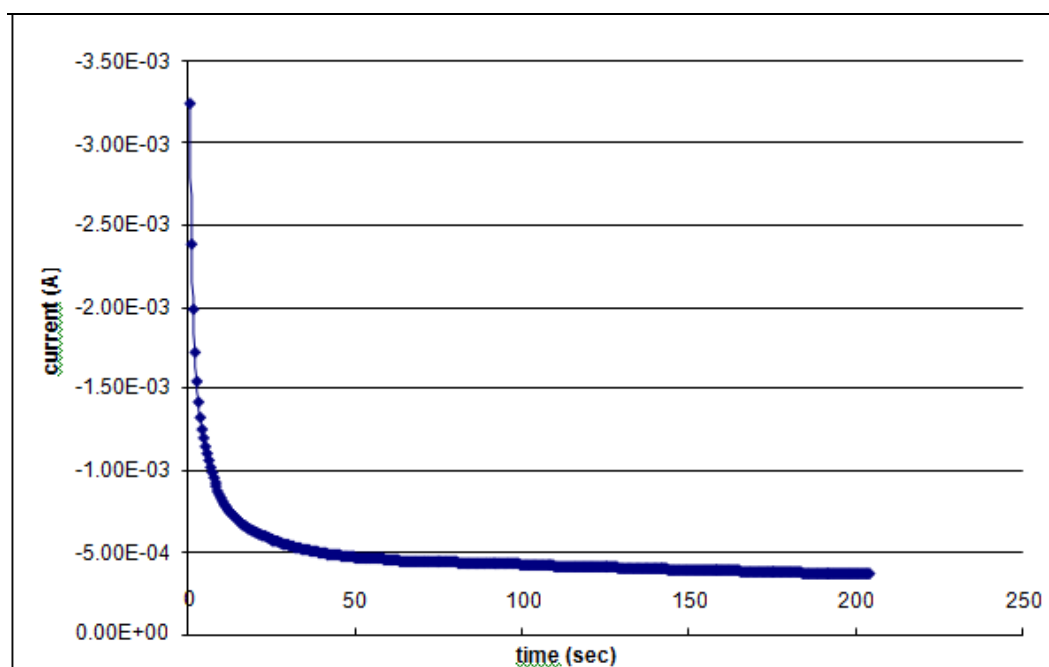


Fig 3.17: Current vs. time data for the deposition of gold.

The steady state current for the gold deposition corresponds to a current density in the range:

$$3.27\text{mA}/\text{cm}^2 < I_d < 9.09\text{mA}/\text{cm}^2$$

which lies within the optimal current density range for this plating solution (1.1 – 10.8mA/cm²).

TEM images of the resulting nanoparticles (fig 3.18) show that, in addition to the presence of fragments of the chromium adhesion layer, nanorods with an unexpected hybrid structure are formed under these conditions, consisting of a solid segment with what appears to be a rod-like “tail” of porous material. EDAX analysis (fig 3.19) of these particles confirms that they consist entirely of gold, while high resolution TEM images of the nanorods confirm the porous nature of the “tails”, and suggest that the gold deposits have a polycrystalline structure (fig 3.20).

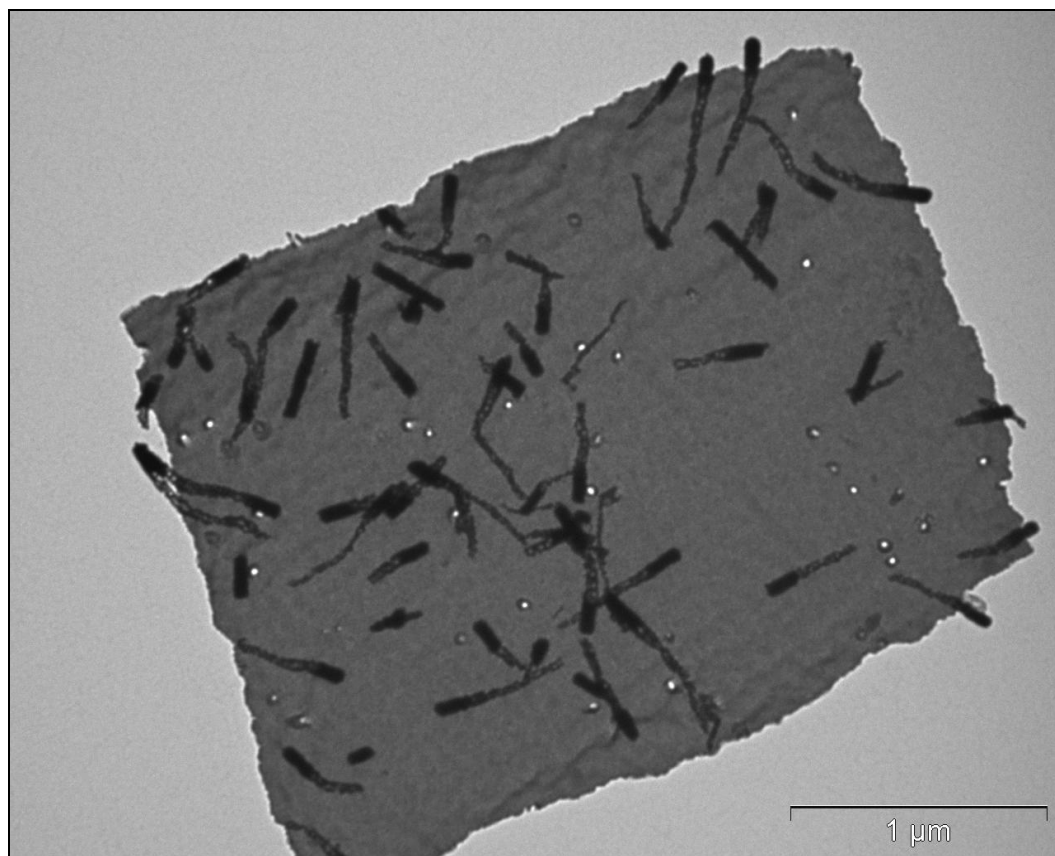


Fig 3.18: TEM image of Au nanorods synthesized under literature conditions.

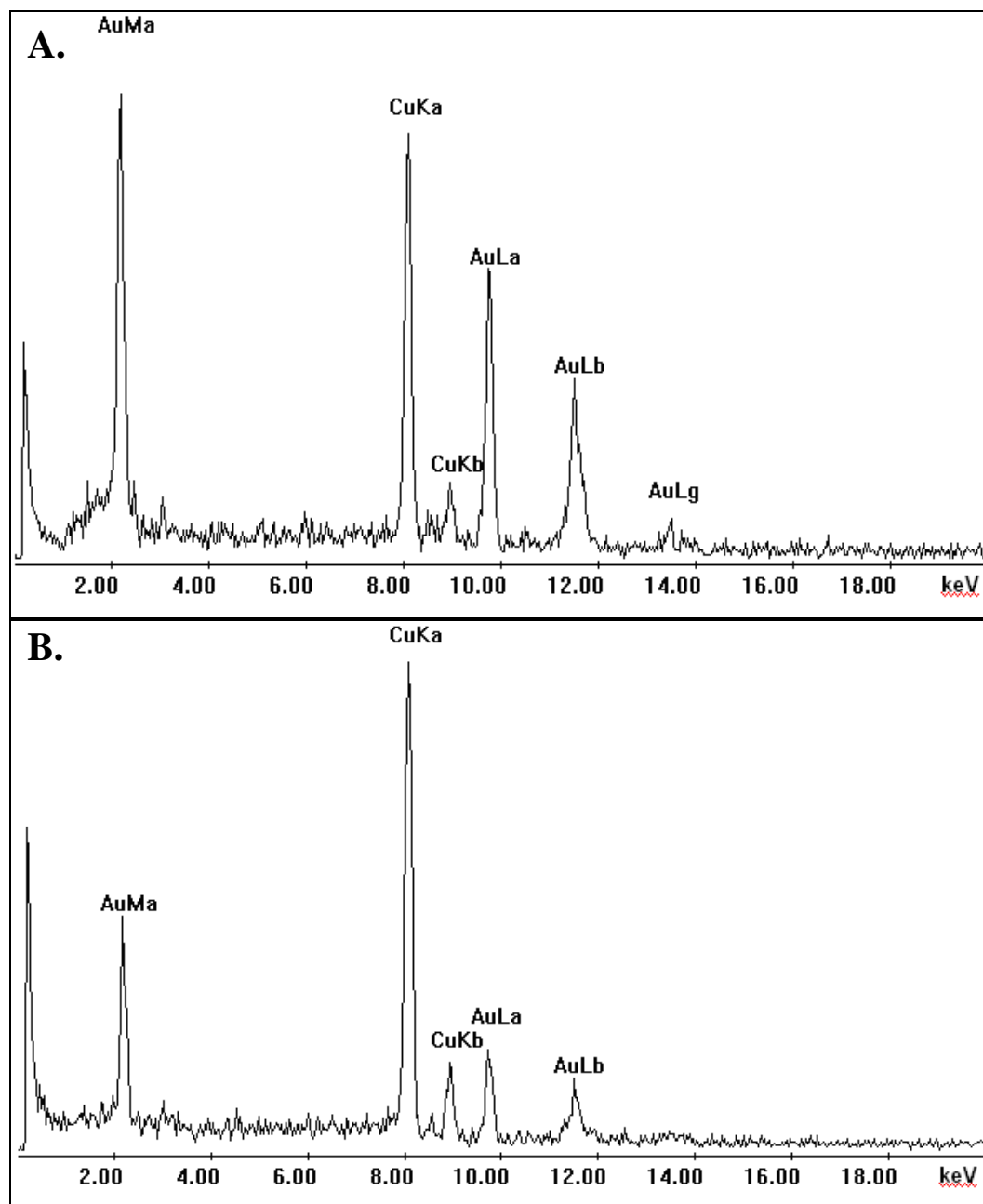


Fig 3.19: EDAX spectra of (A) the solid nanorod segments and (B) the porous "tails".

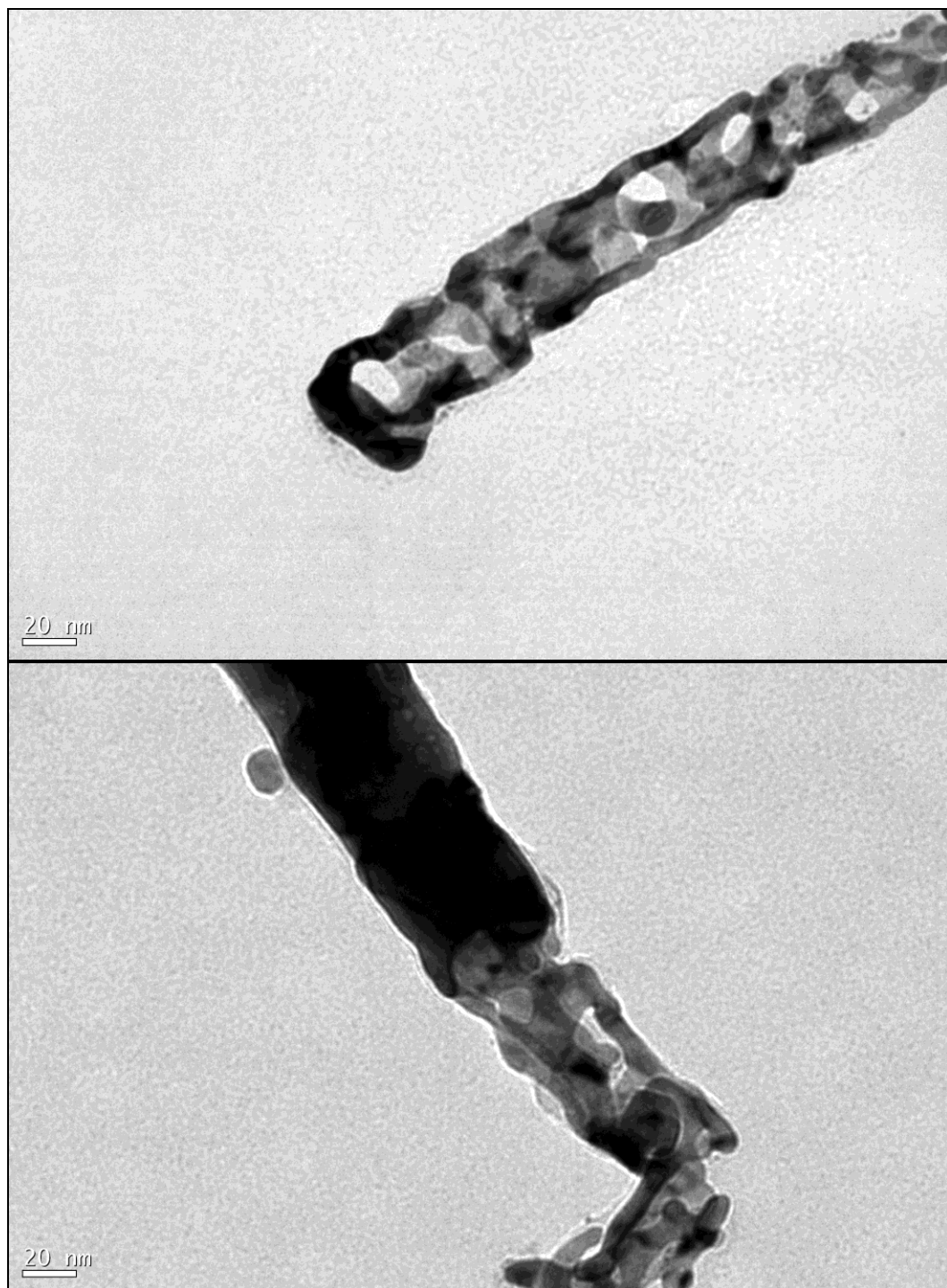


Fig 3.20: High resolution TEM images of (a) porous gold "tails" and (b) solid gold nanorod segments.

In order to explain this result, several possibilities were initially considered. Firstly, it was considered that the current density during electrodeposition of the gold may have been high enough that hydrogen gas was evolved at the cathode, with the resulting bubbles remaining trapped in the narrow membrane pores, thereby creating voids in the deposited gold.[29] However, this was ultimately deemed to be unlikely here, as the calculated current density during deposition of the gold is well within the limits for highly current efficient gold deposition from this plating solution. [30]

A second possible explanation is that these structures are in fact incompletely formed gold nanotubes, which can come about due to the reduction of gold species that are preferentially adsorbed on the walls of the membrane pores. [29, 31] This explanation was contemplated as the prevailing conditions during the gold deposition, namely low overpotentials (the reduction potential of gold cyanide is -0.6V vs. Ag/AgCl [32]) and a low gold concentration near the cathode (current vs. time data in figure 3.17 indicates diffusion limited growth – a result of the long narrow membrane pores and negatively charged gold species), are conducive to the formation of such gold structures. [29] In order to test this explanation, syntheses were carried out with varying amounts of gold being deposited into the membrane pores (25 and 100mC), as the growth mechanism of these structures involves the formation of long nanotubes, followed by inward growth into nanorods. Thus, if this explanation is correct, deposition of greater quantities of gold should first yield longer nanotubes, followed by thicker nanotubes that ultimately grow into solid nanorods, while deposition of less gold should yield shorter nanotubes. [29] However, although TEM imaging (figure 3.21) shows that depositing less gold does indeed yield only porous nanotube type structures, deposition of more gold instead yields nanorods with longer solid gold segments.

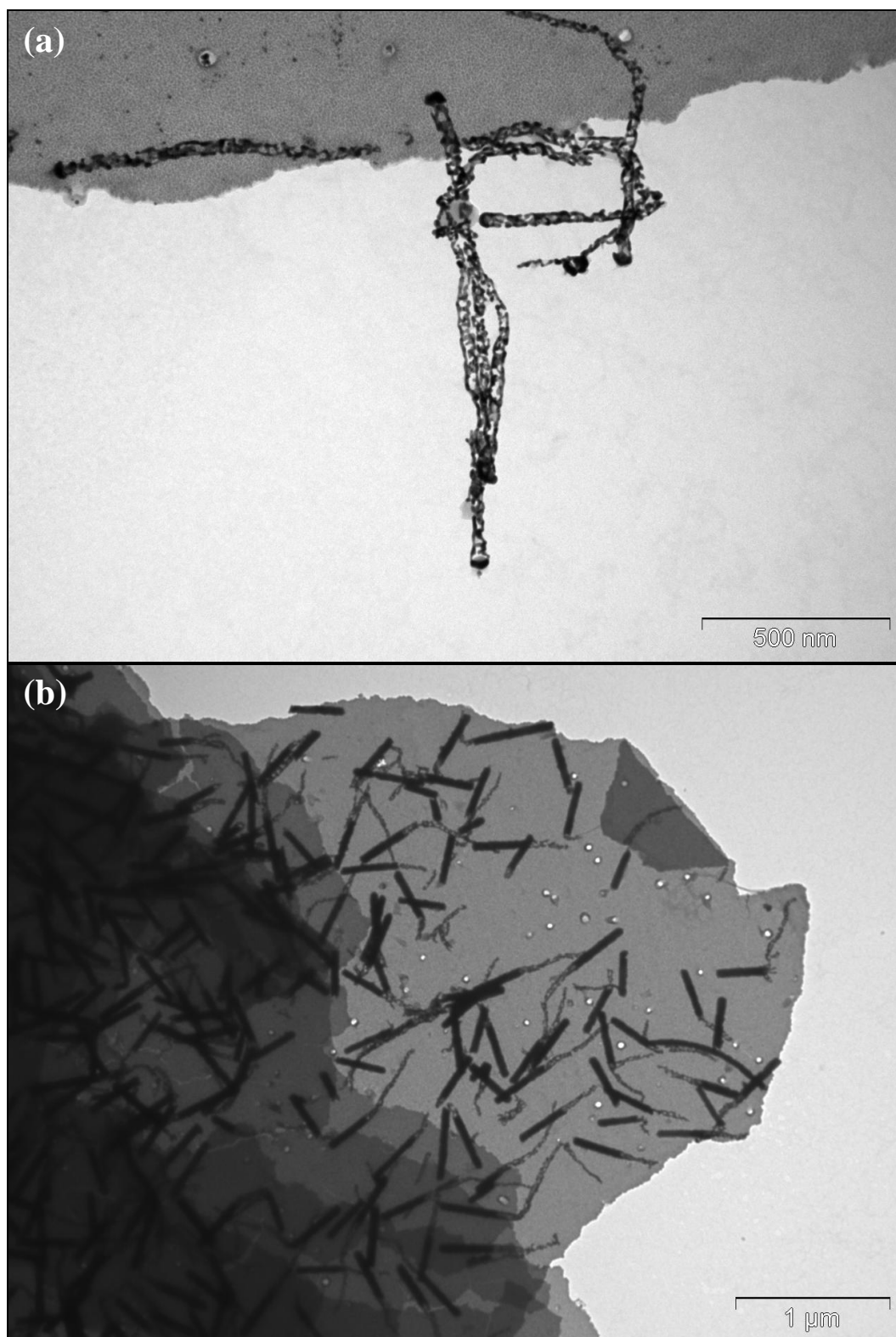


Fig 3.21: TEM images of Au nanorods formed with a passed charge of (a) 0.025C and (b) 0.1C.

Based on this result, it was then hypothesised that these porous gold structures may be due to co-deposition of the gold with impurities, most likely residual silver species from the previous plating solution. This would account for the formation of both the porous segments (coarsening of the gold upon chemical removal of the silver from the resulting gold-silver alloy [33-39]) and the additional solid gold segments upon further gold deposition (residual silver species are eventually depleted yielding only gold deposition). To test this explanation, TEM images were collected of nanorods (50mC of charge passed) prior to treatment with nitric acid (figure 3.22). As predicted, nanorods with two distinct segments are present; a solid gold segment (**A**), and a lower electron density segment that is confirmed by EDAX to be comprised of a mixture of both gold and silver (**B**).

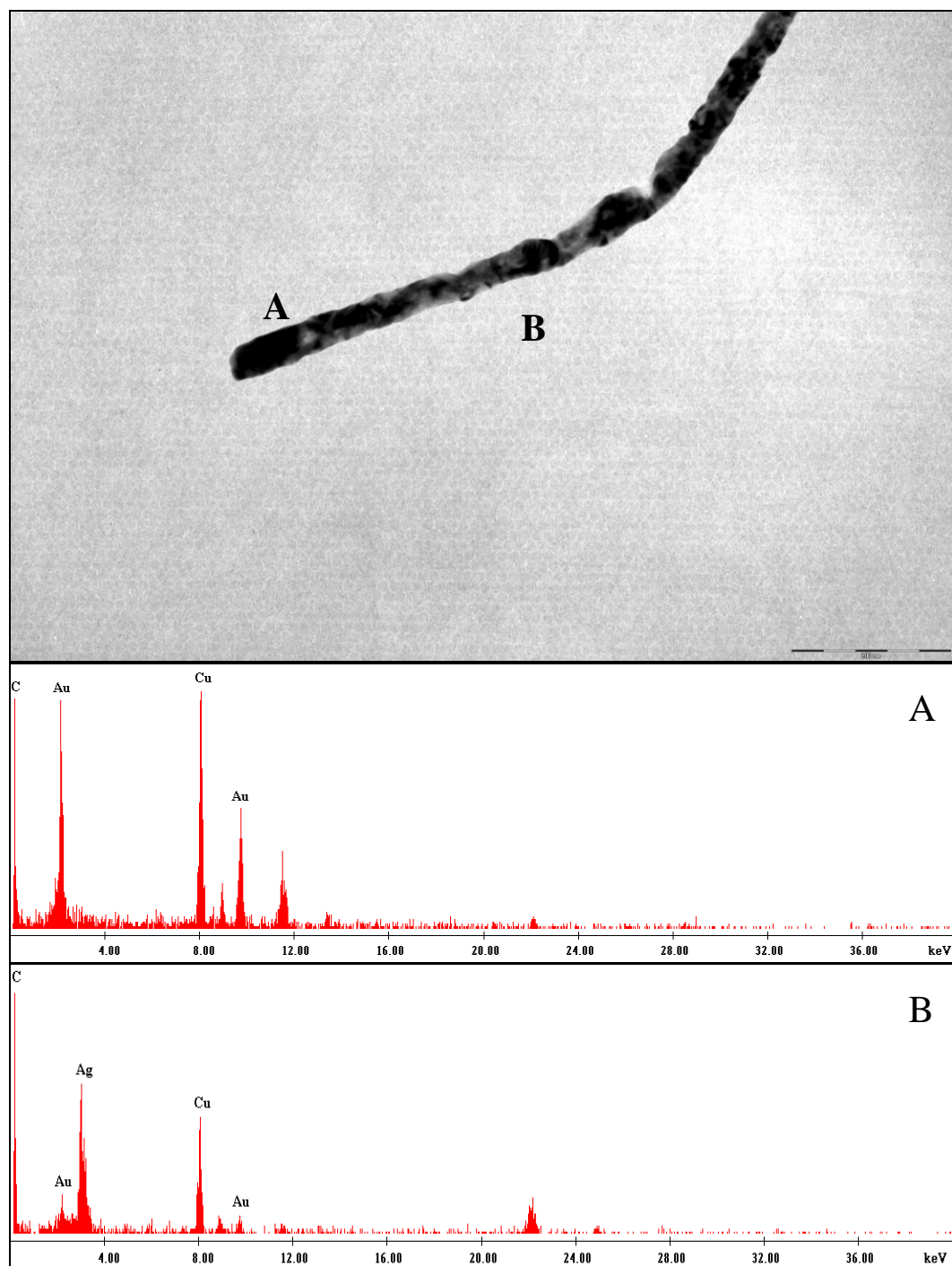


Fig 3.22: TEM image of an Au nanorod without nitric acid treatment (bottom) EDAX spectra of (A) the left segment and (B) the right segment.

Discussion

The template electrodeposition of nickel and gold into the pores of polycarbonate membranes to form nanorods was successful, using current densities within the optimal range for the most current efficient deposition. Both nickel and gold depositions occurred by a mass transport limited process, likely owing to the narrow pores through which the metal species must pass to be reduced at the cathode. The nanorods also formed with a wide range of segment lengths. The formation of porous gold nanorods, owing to the nitric acid etching of residual silver species that are codeposited with the gold, indicates that the most commonly used method for removal of residual metal species from the pores is ineffective in the case of these small pore diameters. Interestingly, despite the presence of this residual silver in the pores, the nickel nanorods formed in the initial experiments exhibit no signs of codeposition with silver (as was the case with gold). This absence of codeposition is confirmed by TEM images (and EDAX) of nickel nanorods that are synthesised and collected without treatment with nitric acid (fig 3.23). This difference is believed to come about due to differences in the standard reduction potentials of the metal species in the given solutions. [40] In the case of the nickel deposition, residual silver is preferentially reduced over the nickel due to its much greater reduction potential, and so is effectively depleted before nickel deposition commences. ‡ Although a similarly large difference in reduction potential exists between the silver and gold species, initial reduction of the gold yields free cyanide in the cathodic diffuse double layer, which complexes with silver species in the vicinity of the cathode to form silver cyanide. Silver cyanide has a much lower reduction potential which is

‡ Approximately 1.6V for AgO 32. Schriver, D.F., Atkins, P.W., *Inorganic Chemistry*. 3rd ed. 1999, Oxford: Oxford University Press. compared to -0.61V for the Ni(NH₂SO₃) 41. Myung, N., Sumodjo, P.T.A., Nobe, K. in *Proceedings of the 3rd Symposium on Electrochemically Deposited Thin Films*. 1997: The Electrochemical Society. under the acidic conditions of the nickel plating solution (vs. standard hydrogen electrode).

similar to that of the gold cyanide species, and so leads to codeposition of both species with no significant preference for one metal over the other. [42] [§]

In these trial experiments, it was also confirmed that the selected silver plating solution chemically attacks the polycarbonate membranes that are used as synthesis templates for the nanorod formation. However, this chemical attack is not anticipated to be an issue in this work, as examination of the nanorods formed in the trial electrodeposition experiments showed that they have diameters ranging between 30 - 50 nm, which compares well with the mean in-depth pore diameter of ~ 40 nm as stated in the literature. Although this range includes nanorods with diameters greater than desired, a significant portion of the nanorods have diameters that are suitably small enough for template directed alignment using the available block copolymer templates.

[§] Approximately -0.31V for $\text{Ag}(\text{CN})_2$ compared to -0.6V for $\text{Au}(\text{CN})^-$ under the slightly acidic conditions of the gold plating solution (vs. standard hydrogen electrode). 32. Schriver, D.F., Atkins, P.W., *Inorganic Chemistry*. 3rd ed. 1999, Oxford: Oxford University Press.

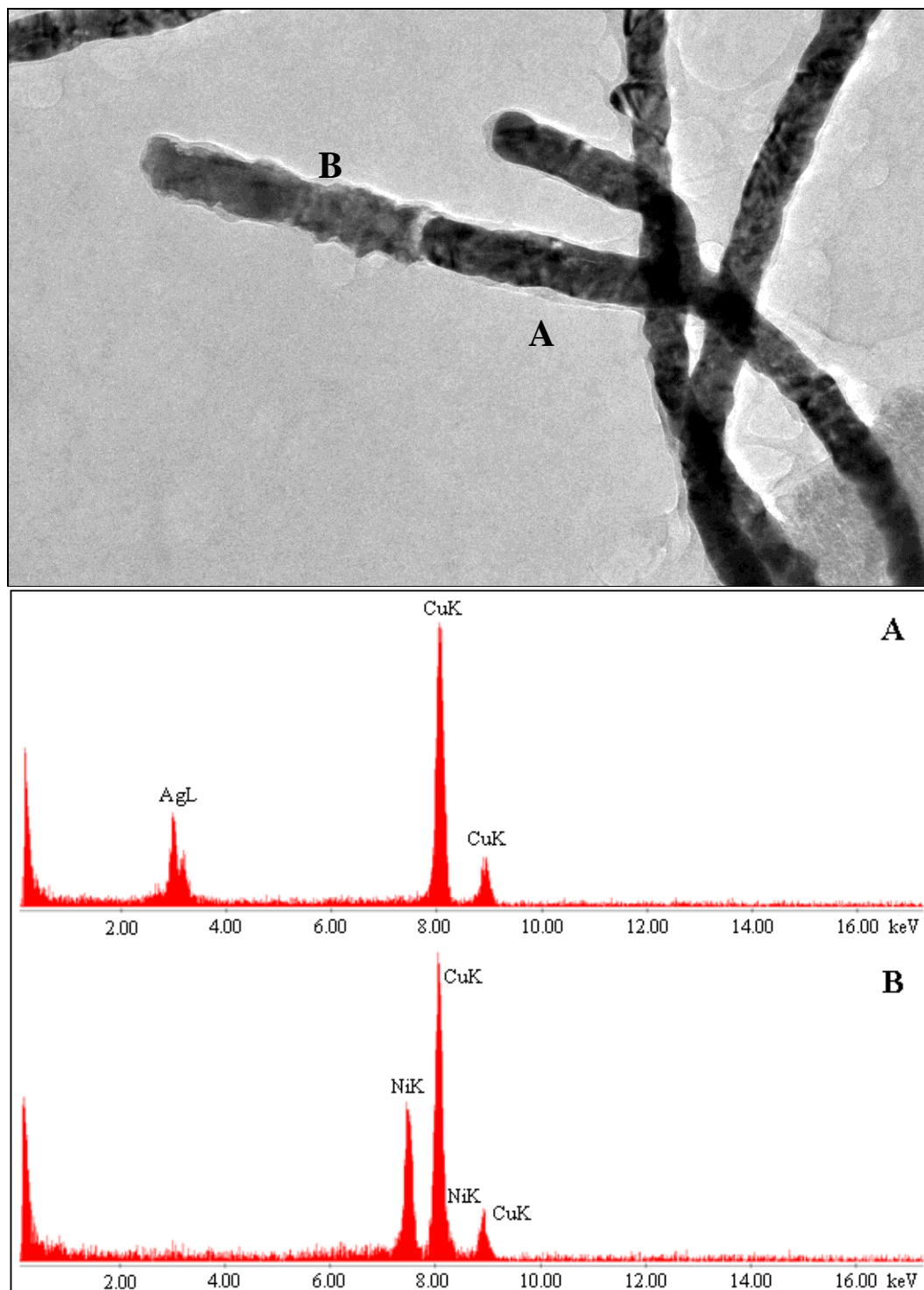


Fig 3.23: TEM image of a Ni nanorod without nitric acid treatment (bottom) EDAX spectra of (A) the right segment and (B) the left segment.

3.3.2. Optimisation Experiments

Based on the results from the initial experiments, a number of further experiments were performed with the aim of optimising the nanorods properties towards that required for template directed alignment of the nanorods using the synthesised block copolymer templates. In particular, experiments were carried out with regards to improving the compositional purity of the nanorod segments, and the distribution of nanorod segment lengths.

3.3.2.1. Composition

As discussed in the analysis of the results of nanorod formation under standard literature conditions, it appears that removal of residual metal species from the membrane pores remaining from previous deposition steps is not readily achieved using the rinsing method commonly used in the literature, so alternative methods for removing such residual metal species need to be investigated and compared if codeposition of the second or third desired metal is to be successful, and any impurities systematically and efficiently removed.

There are a number of ways by which this may be achieved in this work:

- Sonication during rinsing of the membrane to facilitate transport of residual plating solution out of the pores.
- Electrodeposition of the residual plating solution in an electrolyte solution prior to further electrodeposition. [43]
- Deposition of a nickel segment between the deposition of gold and silver.

While the first two methods rely on removal of the residual metal species from the membrane pores, the third method takes advantage of the chemistries of the

respective plating solutions. The deposition of a small nickel segment prior to that of gold effectively removes residual silver from the pores by deposition and replaces it with residual nickel species. Although the reduction potential of the gold and nickel species is rather similar, so one would expect the two metals to co-deposit readily, the pH of the gold solution is high enough that the residual nickel sulfamate species is converted to insoluble nickel hydroxide, thereby removing it from the solution and preventing its co-reduction with gold. [44] The remaining nickel barrier segment may be dissolved by treatment with *dilute* nitric acid (<1M).

Experiments investigating these alternative methods focus on the deposition of gold nanorods, as its deposition appears to be most susceptible to codeposition with the other metals used. The presence of such codeposited metals can also be readily observed by TEM (EDAX). Additionally, the third method is only applicable to the deposition of gold.

Sonication

Following the deposition of the sacrificial silver layer, three consecutive 5 min rinses with nanopure water under mild sonication was done by sealing the glass cell in plastic and immersing the cell in a sonication bath. Subsequent deposition of gold (followed by removal of silver with concentrated nitric acid) yielded gold nanorods consisting of a single solid segment (fig 3.24). The absence of a porous gold segment suggests that sonication in nanopure water is effective in removing residual metal species from the small diameter pores of the membrane.

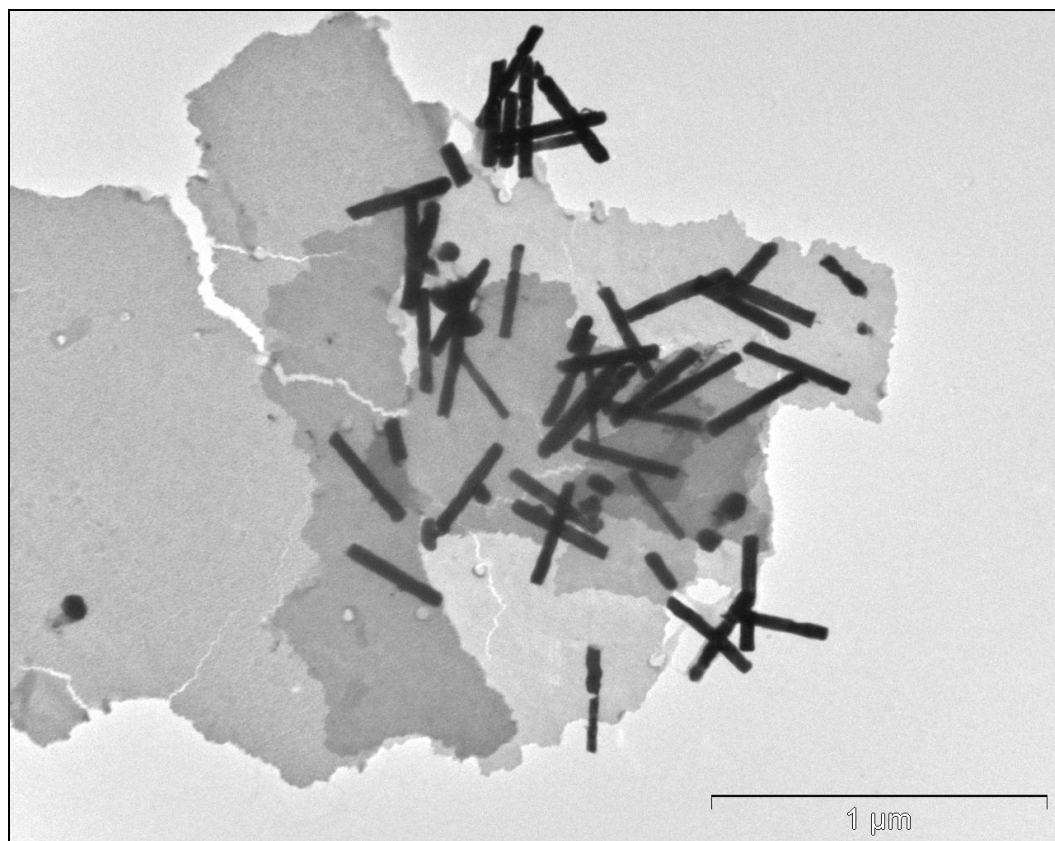


Fig 3.24: TEM image of gold nanorods resulting from metal deposition where rinsing of the membrane between depositions is accompanied by mild sonication.

Electrodeposition

Electrodeposition of the residual metal species was performed prior to rinsing with water by applying a potential of -1.0 V vs. Ag/AgCl between the electrodes in a 1mM KOH (pH 11) electrolyte solution. A *basic* electrolyte solution was used in order to assist in the electrodeposition of the silver species, by (a) lowering the reduction potential of the silver species [32] and (b) reducing the net positive charge of the pore interior surfaces (the polyvinylpyrrolidone surface coating maintains an increasing positive charge with decreasing pH) so that electroosmosis has a much weaker effect on the mass transport (here the electroosmosis acts to transport species out of the pores). [45] These measures were deemed necessary as the low concentration of the metal species will act to greatly reduce the rate of mass transport to the cathode surface by diffusion. Note

that the polycarbonate membranes are virtually unaffected by the pH 11 KOH solution (as shown in fig 3.25) even after exposure for a relatively significant period of time (1 hour vs. the usual several minutes of exposure during electrodeposition of the residual metal species).

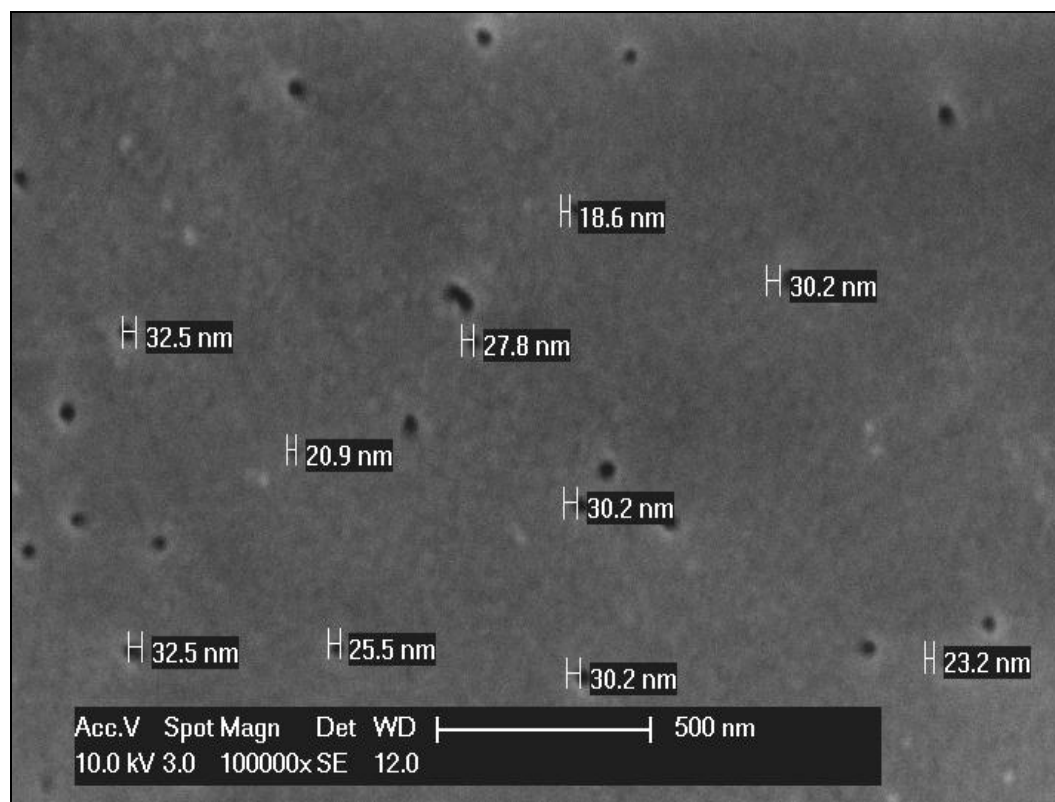


Fig 3.25: SEM image of the surface of a track etched polycarbonate membrane after exposure to pH 11 KOH solution for 1 hour.

Current vs. time data for the deposition of the residual metal species (fig 3.26) shows the characteristic drop in current associated with the establishment of the electrical double layer, followed by a continued steady drop in current as the residual metal species in the pores are reduced (thereby depleting the supply of remaining metal species). TEM images of nanorods resulting from subsequent deposition of gold (fig 3.27) show that porous gold segment formation is largely prevented.

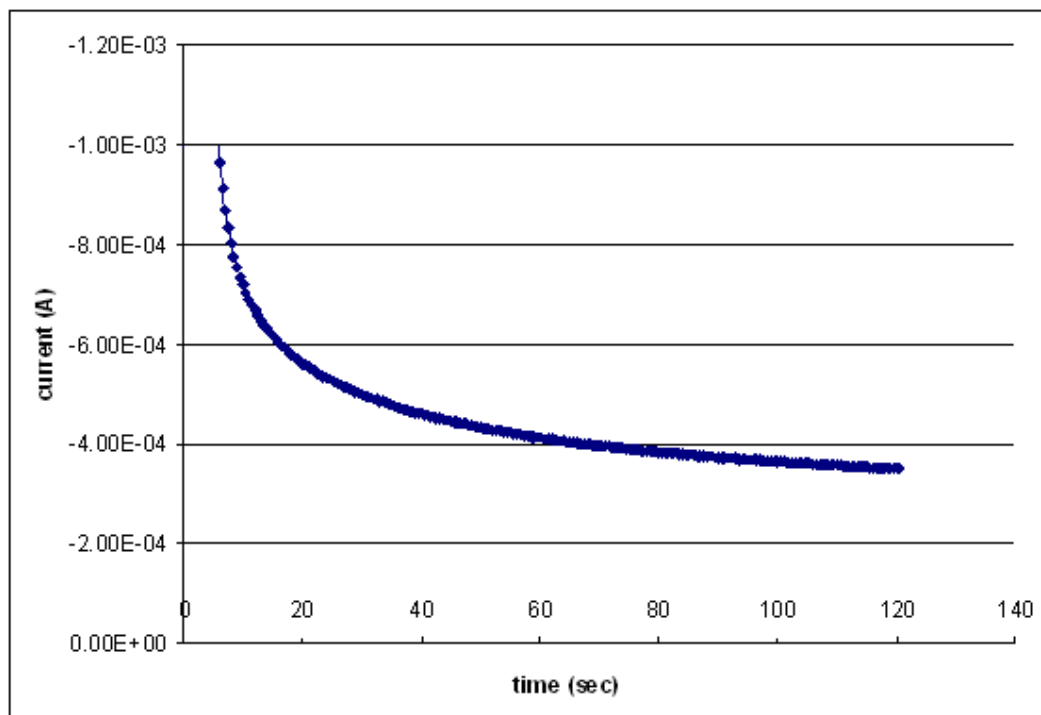


Fig 3.26: Current vs. time data for the electrodeposition of residual silver species in a KOH electrolyte.

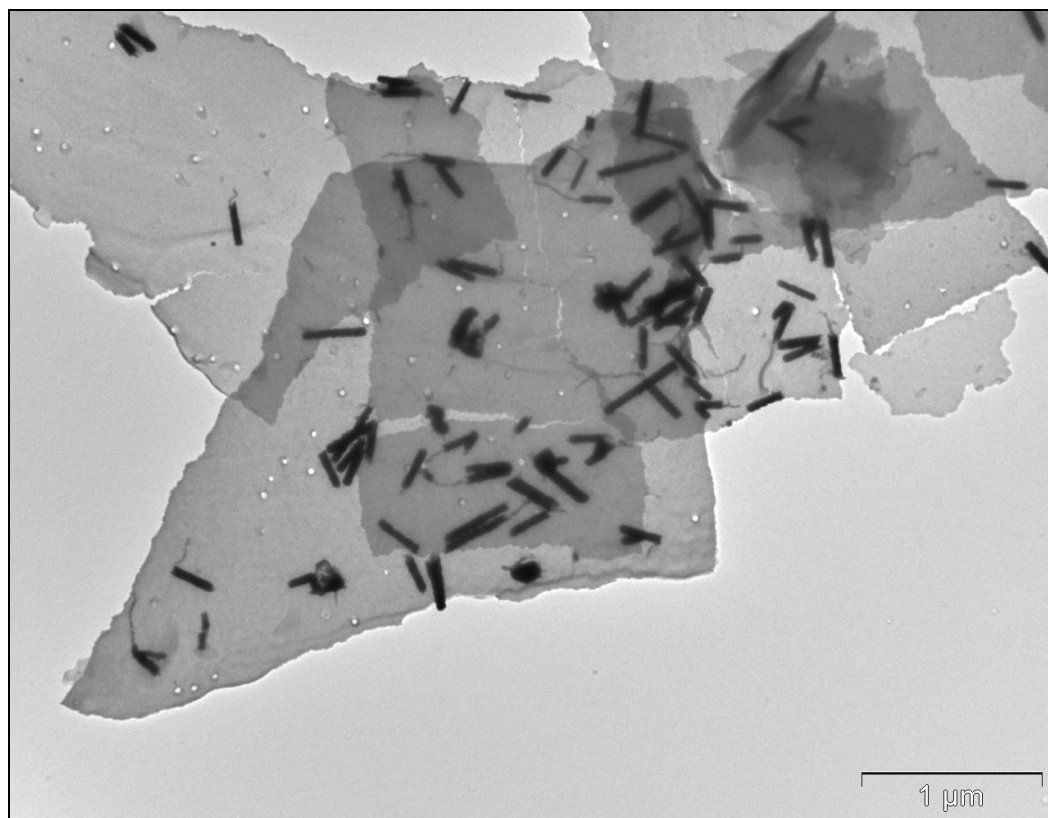


Fig 3.27: TEM image of gold nanorods formed following the electrodeposition of residual silver species.

Nickel Barrier Layer

Deposition of a nickel segment (0.1C) prior to the deposition of gold (0.1C) was carried out using the standard literature conditions as described in section 3.2.2. TEM images of the resulting nanorods (fig 3.28a) show that the nanorods consist of well defined, solid segments (gold) with comparatively low electron density tails (most likely the nickel barrier layer segments that have been attacked during the nitric acid treatment). EDAX analysis of the electron dense, solid segments (fig 3.28b) exhibits strong signals due to gold and the copper TEM grid, with no signals characteristic of either nickel or silver being distinguishable above the background.

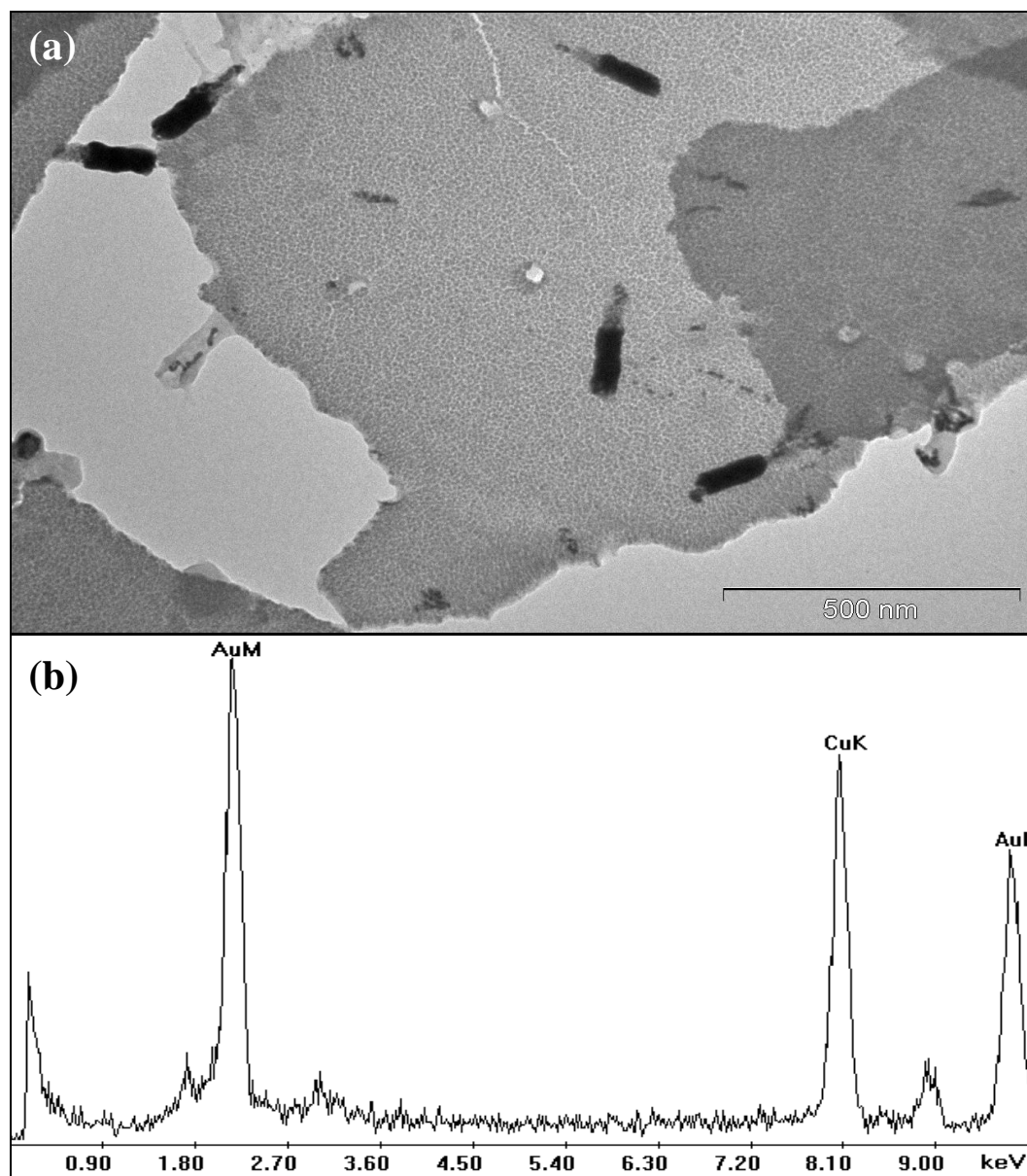


Fig 3.28: (a) TEM image of gold nanorods formed following deposition of a nickel barrier segment (b) EDAX analysis of the gold segments showing the gold Ma and La peaks and the Ka peaks due to copper.

Summary

Overall, each of the methods examined for obtaining metal nanorod segments with pure composition were successful. Sonication of the membrane in nanopure water lead to removal of essentially all of the residual metal species, and appears to be a promising method for application to future experiments involving multi-segment nanorods. Likewise, deposition of nickel prior to the deposition of gold also appears to yield effectively compositionally pure nanorod segments by virtue of the difference in reduction potentials of the metals involved. Removal of metal species by electrodeposition appears to have been largely successful, although deposition to a greater extent than was carried out in these experiments needs to be performed if all of the residual species are to be removed. While this method appears promising in its application to the production of pure single segment nanorods, its application to the formation of multi-segment nanorods may in fact be detrimental, as the deposition of additional metal between segment preparations will act to reduce control over the nanorod segment length. Although this may not be significant in the case of larger diameter or longer nanorods such as those cases in the literature where this method has been applied, its effect in this work where small diameters and segment lengths are desired is expected to be substantial (particularly given the volume of residual solution that remains in the pores as indicated by the extent of porous gold formation). Thus, in future work, both sonication during rinsing and the order of metal deposition will be utilised to produce compositionally pure metal segments.

3.3.2.2. Nanorod Length Distribution

Based on the results from the initial experiments under standard literature conditions, it is clear that nanorods with a wide range of lengths have been formed. In an effort to synthesise better defined nanorods, a number of experiments were performed to determine the conditions under which such variations in length can be minimised. Such experiments were based on the consideration of a number of contributing factors that were identified from the initial experiments. The first factor is that the polycarbonate membrane pores vary with regards to the pore diameter, leading to concurrent variations in nanorod length for a given amount of deposited metal. The second factor is that the presence of residual plating solution in the pores from previous metal depositions also leads to variation in segment length, as some of the charge passed during the given segment deposition is used in the deposition of the residual metal species, and all pores do not necessarily contain the same amount of residue. [43] Finally, the deposition of both gold and nickel in this work being mass transport controlled means that disparity in the rate of mass transport to the various pore cathode surfaces leads to variations in the amount of metal deposited in each pore, thereby leading to a wide range of nanorod lengths.

The first two contributing factors are considered to be extraneous in this work as variations in pore diameter are intrinsic to the membrane template, and suitable schemes for the removal of residual metal species from the pores have been found. Variation in nanorod length due to differences in mass transport over the membrane however, may be managed through the application of methods that minimise the extent/impact of variations in mass transport into the pores.

There are a number of different ways by which this may be accomplished:

- Apply a uniform electric field over the entire membrane.
- Increase the rate of mass transport into the pores.
- Reduce the rate of metal deposition.

The first scheme accounts for variations in electric field strength over the membrane, which leads to differences in the strength of associated mass transport mechanisms and thus, acts to decrease control over nanorod length. Although the electric field is expected to be uniform over the majority of the membrane (due to the cathode being placed at a relatively large distance from the cathode), the electric field strength is in fact much greater at the edges of the cathode [46-48], which leads to visibly greater deposition of metal at the cathode edge due to the greater degree of field driven mass transport (fig 3.29). This variation in electric field strength may be accounted for either through the use of a conical counter electrode, or by removal of the outermost portion of the membrane that contains these nanorods prior to dissolution of the membrane to retrieve the nanorods.

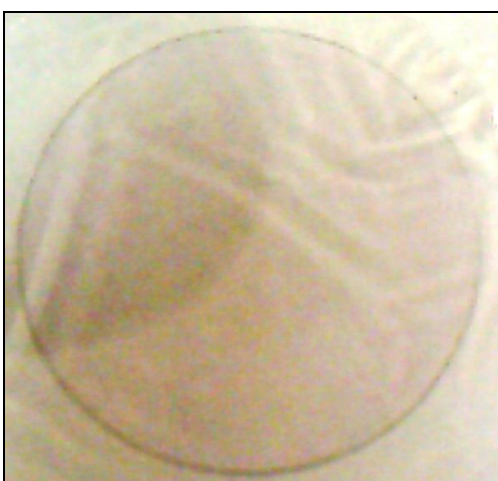


Fig 3.29: Photo of a polycarbonate membrane containing gold nanorods (after nitric acid treatment). Note the visibly preferential deposition at the edge of the deposition area.

The second and third methods concern mitigation of the effect of differences in mass transport over the membrane due to variation in pore diameter. The first of these two methods accomplishes this by increasing the rate of mass transport by advection (instigated by sonication) such that deposition is no longer limited by mass transport. [8] The second of these two methods performs the same function, but achieves this by reducing the rate of metal deposition, so that the nanorod growth is no longer mass transport limited (Tafel behaviour). The most direct way of reducing the rate of deposition is to lower the overpotential, which may be accomplished by directly lowering the potential applied between the electrodes for the metal deposition. However, the exact relationship between the potential and current (rate of deposition) for this system is not known, and would require a significant amount of work to establish for all of the metals to be deposited. A quicker and easier alternative is to impose an *external current limit* on the system by the electrochemical apparatus (through increasing the internal circuit resistance such that currents higher than some pre-defined value cannot pass). This leads to more of the applied overpotential working towards overcoming this resistance, thereby reducing the electrode polarisation (first concentration polarisation and then activation polarisation) and hence the rate of reduction. In this work, the current limit is imposed by setting a current sensitivity for the electrochemical analyser.

Experiments investigating the effect of these methods are focussed on gold nanorods, as the deposition of this metal appears to be most sensitive to the mass transport limitation. Nickel nanorods are not examined as the influencing factors causing differences in mass transport over the membrane are the same for both metals. The gold nanorods are synthesised using a combination of sonication during rinsing between deposition steps along with deposition of a nickel barrier layer to ensure that pure gold nanorods are obtained. All nanorods in a given experiment are synthesised with the same amount of passed charge so that length distributions are comparable. In order to obtain accurate statistics of nanorod

length distribution, at least 125 nanorod length measurements are collected for any given nanorod sample.

Uniform Electric Field

TEM images of gold nanorods both including and excluding nanorods formed in the outermost deposition area of the membrane templates are shown in fig 3.30 and fig 3.31 respectively. From these images, it is apparent that the inclusion of nanorods formed at the edge of the cathode yields a much greater range of nanorod lengths than when such nanorods are excluded. Analysis of the distribution of nanorod lengths in these samples (fig 3.32) confirms this, showing that both samples have a “core” group of nanorods formed with a relatively narrow distribution of lengths (ascribed to those formed in the bulk of the membrane away from the edge), with a significant percentage (~ 25%) of the nanorods, in samples where the outermost section of the membrane is not removed prior to nanorod collection, being of much greater length. These nanorods are ascribed to the much smaller population of nanorods formed at the edge of the cathode, where preferential metal deposition takes place.

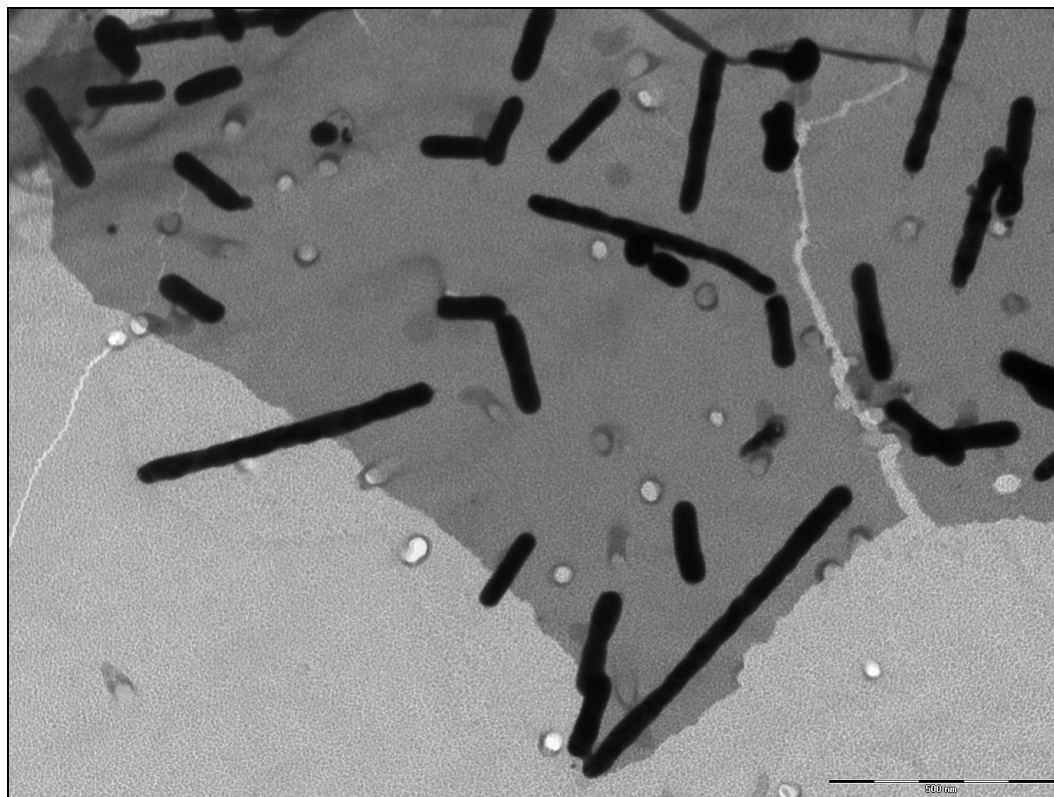


Fig 3.30: TEM image of nanorods including those resulting from metal deposition in the outermost segment of the synthesis template.

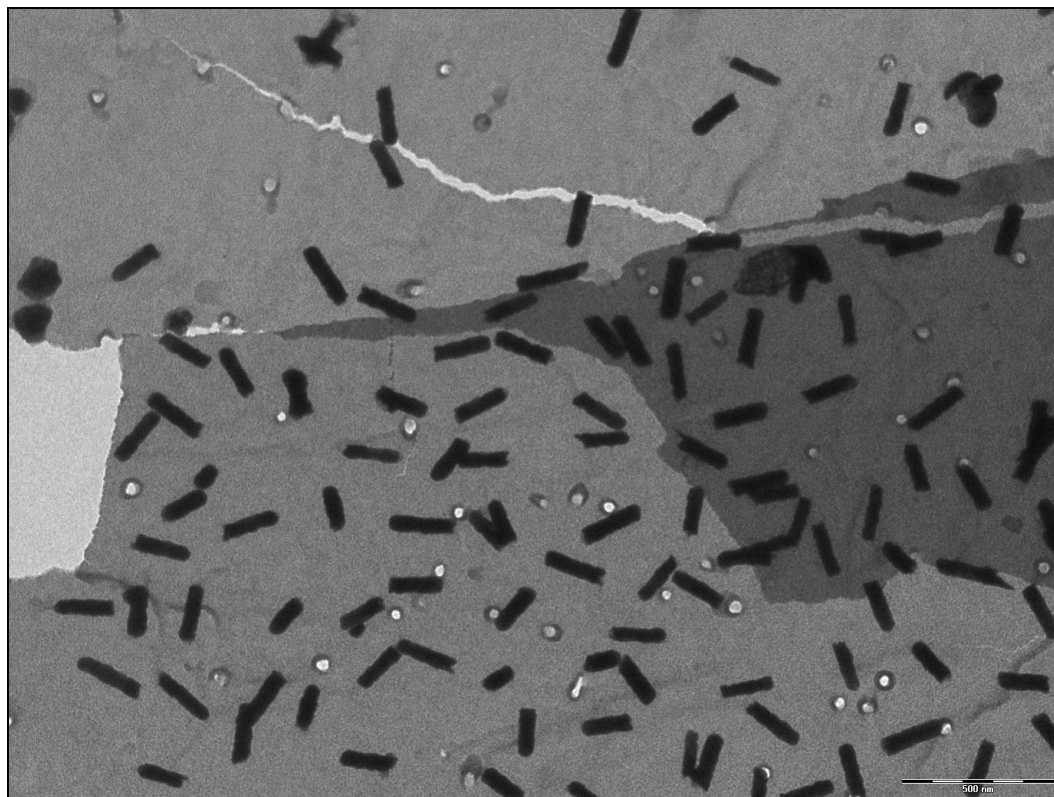


Fig 3.31: TEM image of nanorods excluding those resulting from metal deposition in the outermost segment of the synthesis template.

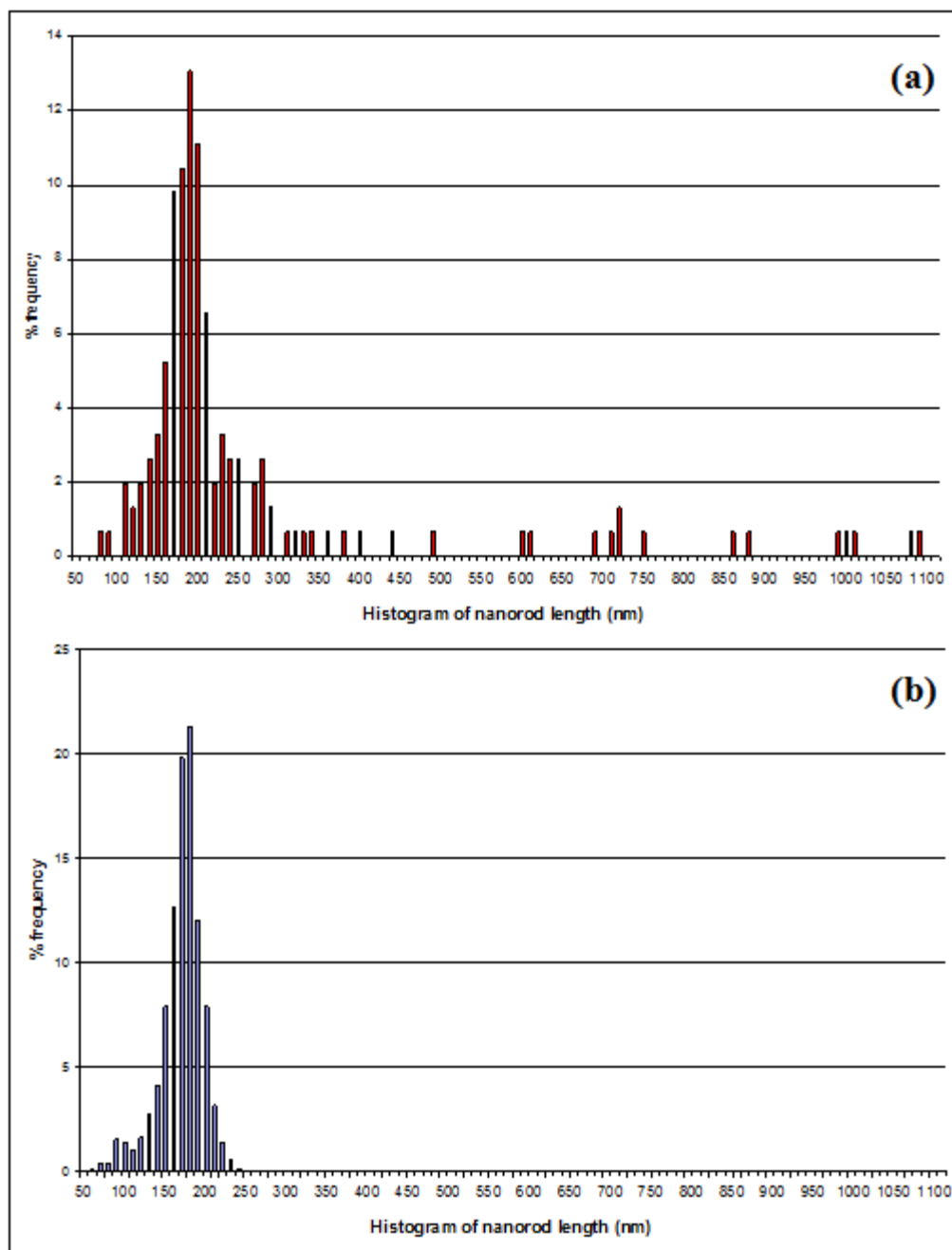


Fig 3.32: Length distributions of gold nanorods (a) including and (b) excluding those formed from metal deposition at the edge of the cathode.

Current limit

The effect of reduced rates of metal deposition upon the length distribution of the nanorods is investigated by comparing three different current limit regimes; (i) no limit, (ii) 1 mA limit and (iii) 0.1 mA limit. Deposition at these limits yield current densities within the acceptable range for optimal current efficiency, yet they remain lower than the highest current reached during electrodeposition under standard conditions. Note that for all of these samples, the outer edge of the membrane is removed prior to nanorod collection and imaging.

A comparison of the length histograms obtained for the deposition of gold to form nanorods under a current limit of 1mA and no current limit is shown in fig 3.33. As can be seen, the nanorods resulting from deposition under a 1mA current limit appear to have a much narrower distribution of lengths (standard deviation of 26.1nm) compared to when no current limit is applied (standard deviation of 64.4nm). Interestingly, this occurs despite the fact that the limiting current used in this case is *greater* than the mass transport limited current for gold deposited into these membranes under standard conditions, which would suggest that the deposition is still mass transport limited, and so remains subject to the effects of mass transport variations over the membrane.

This result may be explained by considering that, initially, the faradaic current due to reduction of gold is accompanied by a capacitive current due to charging of the electric double layer, and that the current limit is lower than that which flows from the combination of these currents under standard conditions. Given that both of these processes occur simultaneously and each account for a portion of the observed (limited) current flow [49], the restriction on these combined currents results in (a) the double layer taking significantly longer to charge and (b) the gold reduction occurring at a lower rate than suggested by the observed (externally limited) current. The gold reduction rate during charging of the double layer is most likely lower than that corresponding to restriction by mass transport (as indicated by current vs. time data for this deposition (fig 3.34) which shows

that a drop in current due to the onset of formation of a diffusion layer is delayed significantly), and so a large portion of the metal deposition to form the nanorods occurs without the mass transport limitation, thereby reducing the impact of variation in the subsequent mass transport limited growth of the nanorods.

Nanorods formed under the 1mA current limit are significantly shorter (mean length of 165.1nm) than when no current limit is applied (mean length of 259.1nm), despite the fact that the same amount of charge is passed in both cases, and that no significant difference in nanorod diameters is observed. One explanation for this is that the current density during the initial charging step is so low that it is outside of the optimal range of current densities for this deposition, leading to a reduced current efficiency. Alternatively, this may simply result from the more even deposition over the membrane.

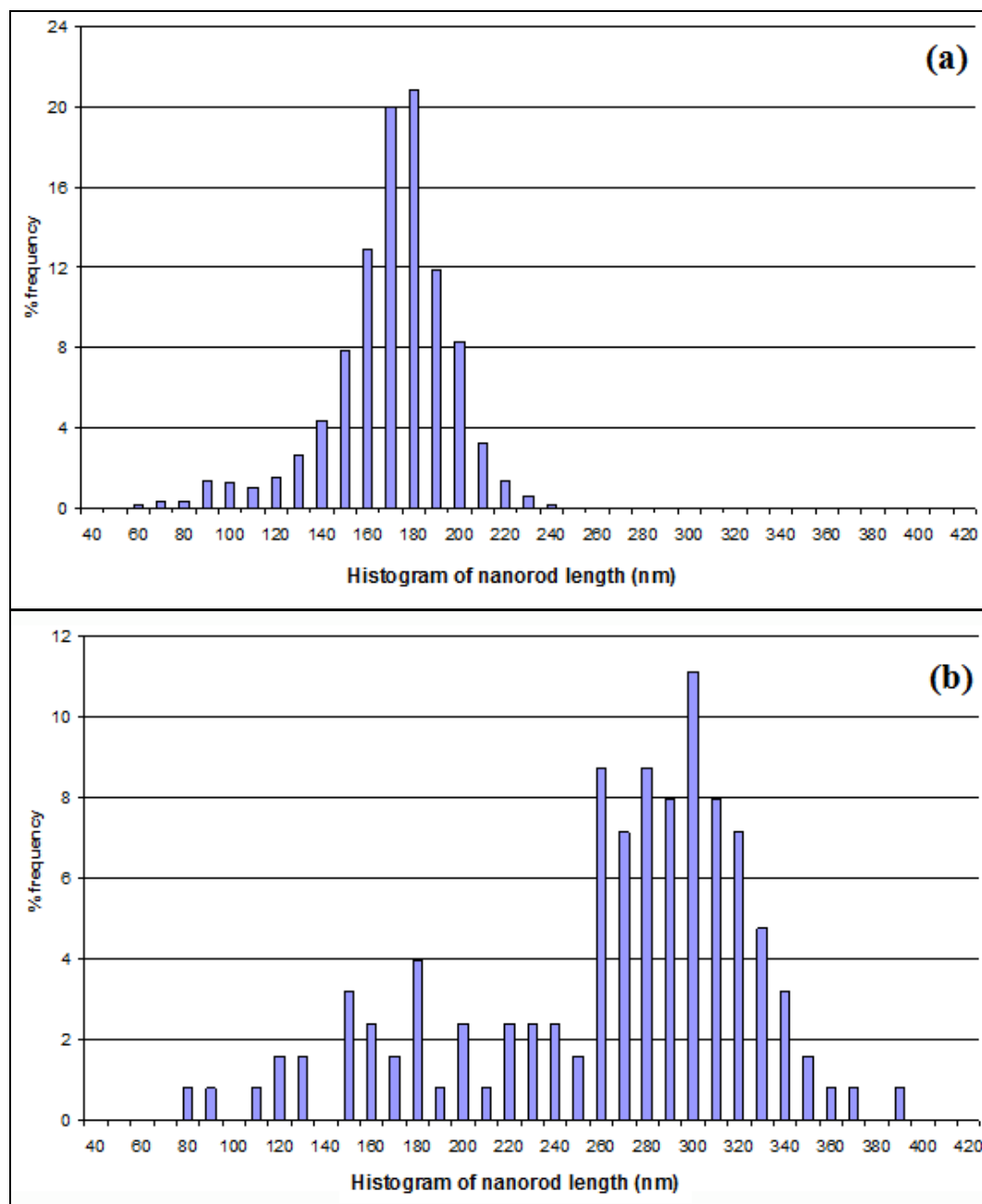


Fig 3.33: Length distribution of gold nanorods formed with (a) a 1mA current limit and (b) no current limit.

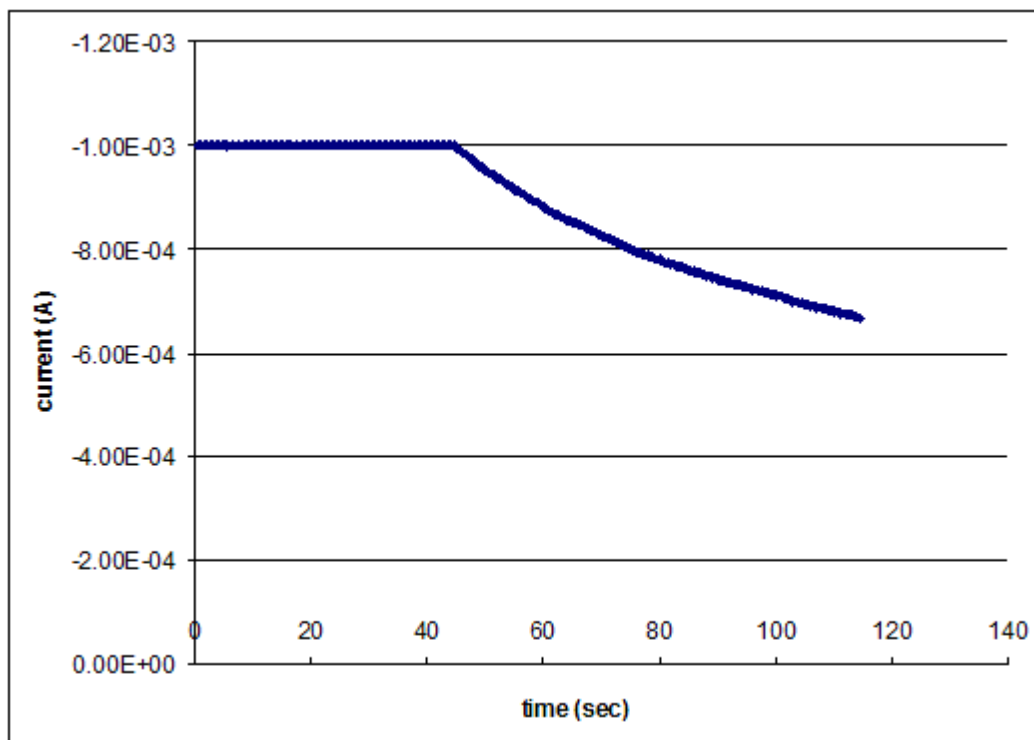


Fig 3.34: current vs. time data for gold deposition at a current limit of 1mA.

Deposition of gold to yield nanorods under a current limit of 0.1mA yields a distribution of nanorod lengths that consists of a “core” distribution (representing the majority of the nanorods) that is similar to that obtained for nanorods formed under a current limit of 1mA (but that is a little narrower and has a smaller mean length of 141.9nm), along with a low, extensive tail towards longer nanorods (yielding a total standard deviation of 42.5nm) (fig 3.35).

The narrower core of the length distribution is attributed to the fact that the current limit is less than that corresponding to deposition under the mass transport limitation, causing the deposition to proceed slowly enough so that no mass transport limitation occurs during the electrodeposition. The origin of the small population of anomalously high length nanorods in this distribution is unknown, but may result from an effect associated with the rather low electrode polarisation used in this deposition (as most of the overpotential is used to overcome the high external circuit resistance). For example, instead of being directly reduced, the deposition of gold from gold cyanide species at such low overpotentials is

mediated by a layer of adsorbed cyanide species, the surface coverage and nature of which may vary between pores. [50-51]

The shorter average nanorod length is rationalised by considering that the slower deposition in this case yields even more uniform deposition over the membrane, or that the charging of the double layer takes even longer in this case (as shown in fig 3.36), such that the lowered current density (and hence lower current efficiency) is prevalent for a longer period of time during this deposition. In addition, it is also possible that the more restricted current yields an even lower current density than is the case for deposition under a current limit of 1mA.

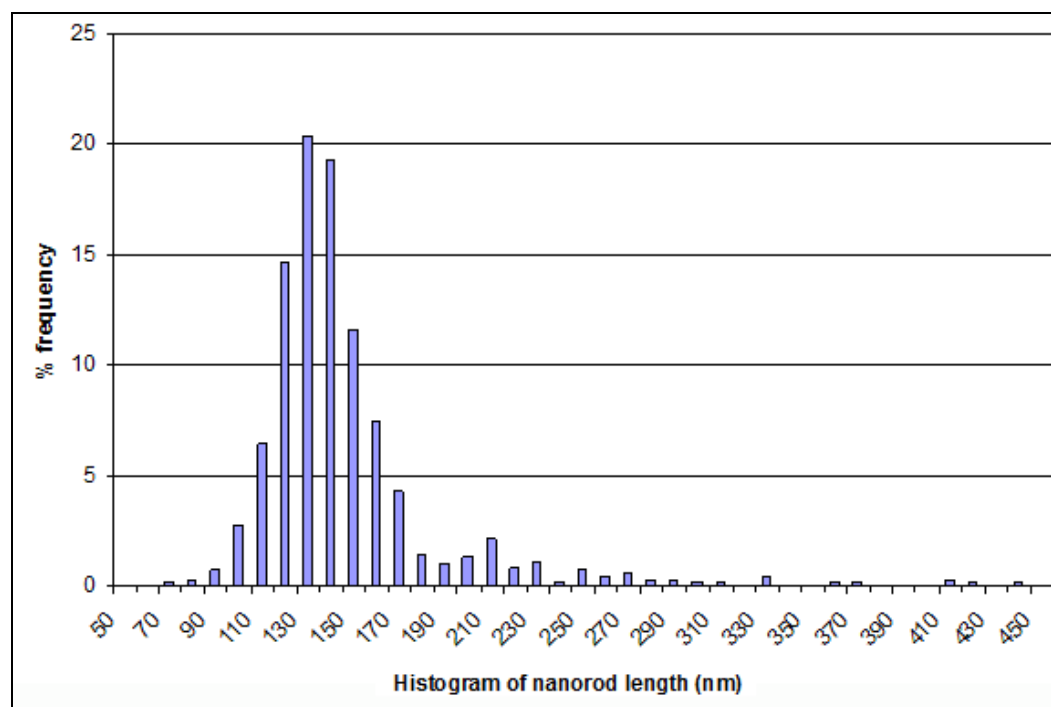


Fig 3.35: Length distribution of gold nanorods formed with a 0.1mA current limit.

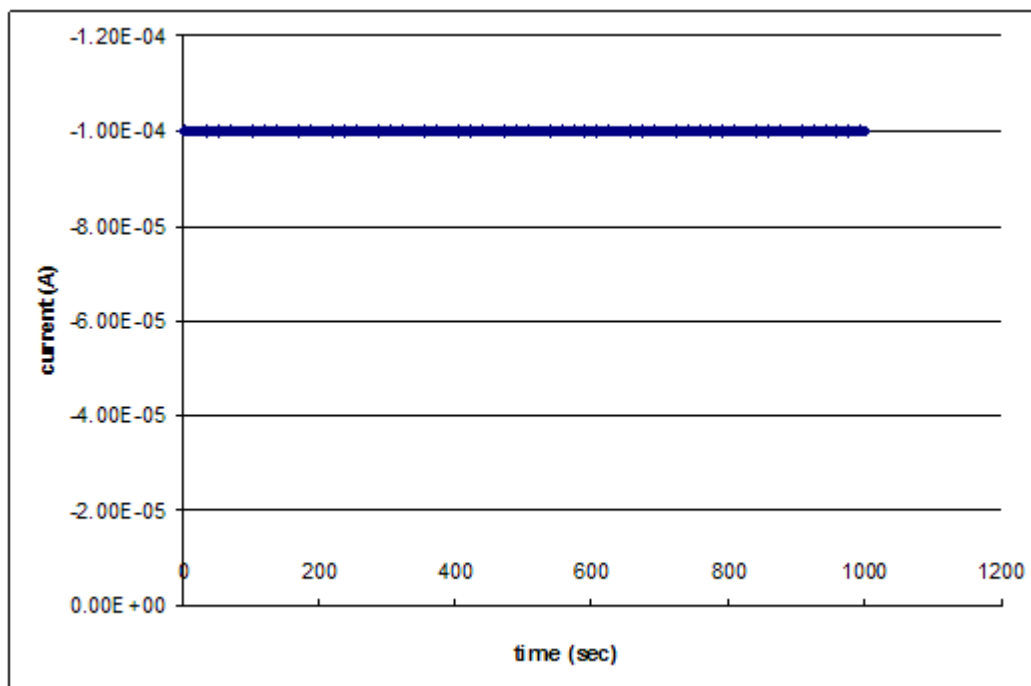


Fig 3.36: current vs. time data for gold deposition at a current limit of 0.1mA.

Sonication

Sonication is performed during deposition of gold to form nanorods in the same manner as sonication during rinsing. Here, deposition occurs under current limited conditions (1mA limit), and the outer edge of the membrane is removed prior to nanorod collection.

The length histogram for the nanorods formed under these conditions (fig 3.37) is very similar to that obtained for deposition under a current limit of 1mA, being somewhat narrower (standard deviation of 18.1nm) and having a smaller mean nanorod length (mean length of 134.5nm). The narrower length distribution is attributed to the improved mass transport that sonication provides (as indicated by the longer time for the diffusion layer to be established in the current vs. time data shown in fig 3.38), while the smaller mean nanorod length is accredited to (a) the resulting improvement in deposition uniformity or (b) disruption of the electric double layer by sonication, which hinders the double layer charging to

equilibrium, thereby requiring more of the total charge passed (note that the current vs. time data also conforms with this latter explanation).

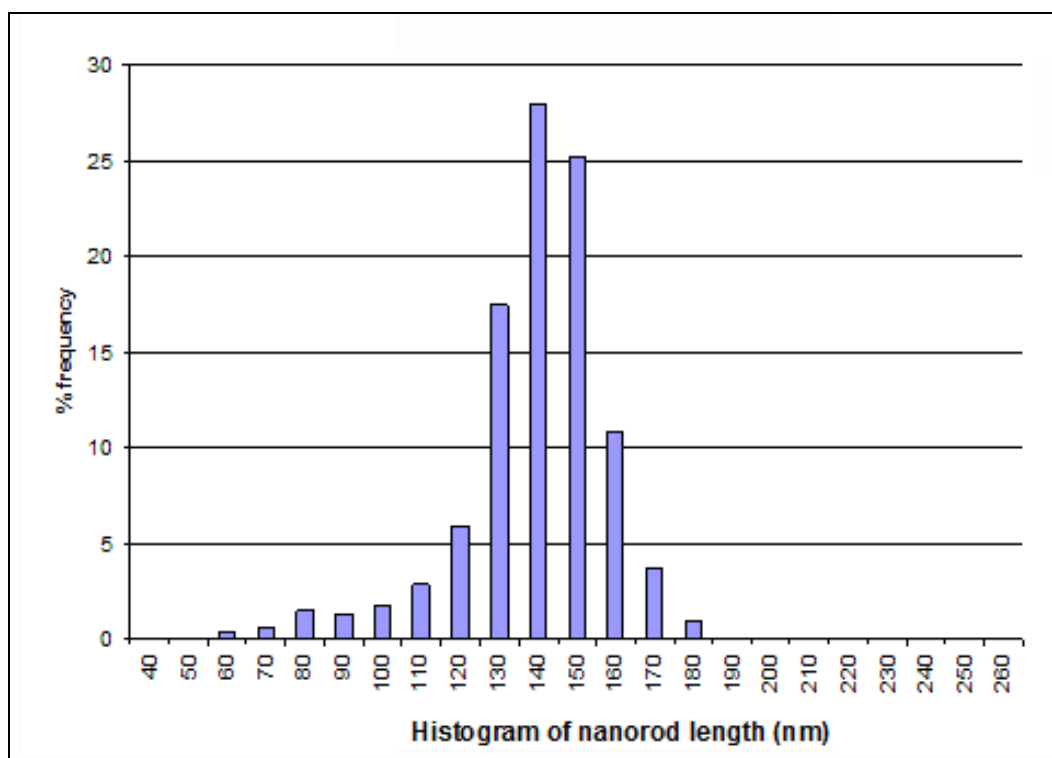


Fig 3.37: length histogram for gold nanorods synthesized under a current limit of 1mA with sonication during the deposition.

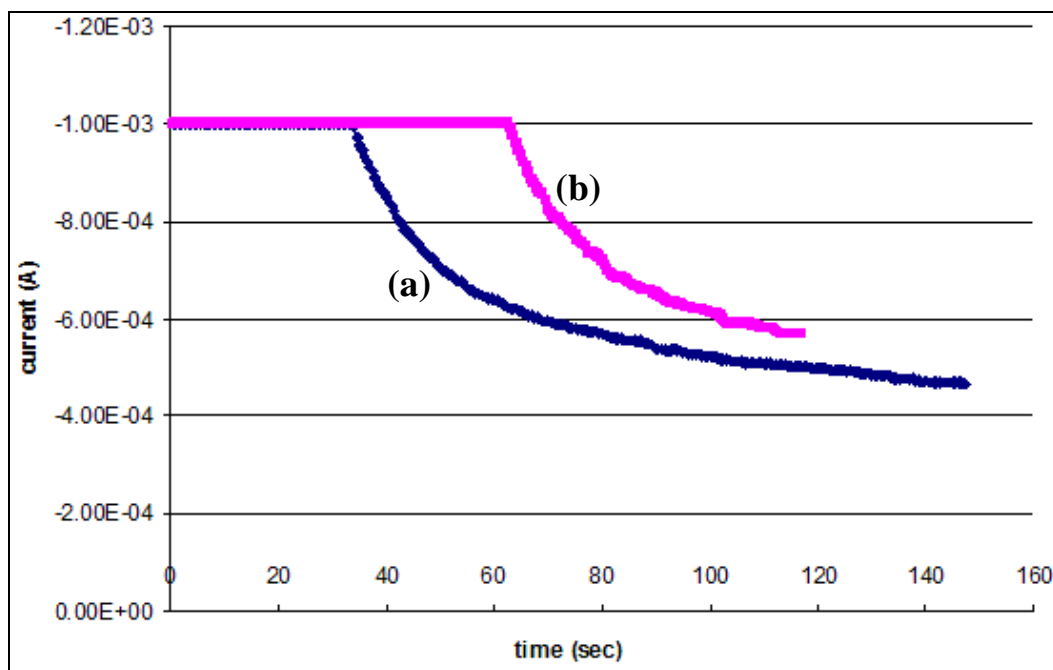


Fig 3.38: current vs. time data for gold deposition (a) under a current limit of 1mA and (b) under a current limit of 1mA with sonication.

Discussion

All of the methods devised to compensate for the differences in mass transport into the membrane pores yield a substantial decrease in the range of nanorod lengths produced (compared to when no such methods are employed). Removal of the outer edge of the membrane template, for example, eliminates the rather long nanorods produced as a result of preferential deposition at the cathode edges. The use of sonication of the membrane during electrodeposition (to increase the rate of mass transport into the pores) on the other hand, was found to significantly reduce the range of nanorod lengths produced, by promoting more uniform deposition rates. Likewise, the application of a current limit was also found to yield a significant decrease in the range of nanorod lengths produced by promoting more uniform metal deposition through limiting the deposition rate. While limiting the current below that corresponding to mass transport limitation under standard conditions predictably yields rather narrow nanorod length distributions (as the deposition is not mass transport limited at any point), it was

found that the use of current limits above that corresponding to mass transport limitation but below that due to double layer charging, also yields a substantial (although somewhat smaller) improvement in nanorod length distribution. Here the restricted charging of the double layer (which necessarily accounts for a portion of the limited current) forces the deposition rate to be decreased below the current limit during this charging time, thereby restricting the impact of the mass transport limitation upon this deposition. While greater current limitation appears to yield the narrowest distributions of nanorod length, there appears to be a limit to the applicability of this method, as at the lowest trialled current limits (where the deposition is slow enough that the mass transport limitation no longer occurs) anomalously long nanorods are formed, possibly as a result of effects associated with the low electrode polarisation (and current density that is in all probability lower than the optimal range) prevalent during deposition under these conditions. Thus, it is judged that moderate current limits (between the currents due to charging and mass transport limitation) are most suitable for obtaining narrow length distributions.

Importantly, it should be noted that these methods appear to be complimentary, each offering a successive improvement upon the length distribution. In particular, the use of moderate current limits only results in part of the deposition occurring at a rate that is not mass transport limited. By also applying sonication, the period of time over which such deposition occurs is extended, thereby yielding still narrower length distributions. As a consequence, all of these methods will be applied so that nanorods with the narrowest distribution of length can be formed.

3.3.3. Nanorod Collection

The effectiveness of the standard literature method of removing the track etched polycarbonate template and collecting the nanorods was evaluated by examination of TEM images of nanorod samples prepared under standard conditions. Note that the chromium adhesion layer is not placed on the membranes in these experiments, as the chromium fragments adhere to the nanorods (as observed in TEM images from previous experiments), and so will influence (reduce) the rate of sedimentation of the nanorods during collection by centrifugation.

As shown in the TEM of figure 3.39, the nanorod samples collected using the standard method are observed to contain a large amount of low electron density material that is confirmed to be absent from the neat TEM grids. Two forms of residue are noted; broad smears of material (less prevalent) that is commonly seen adhering to the surfaces of the nanorods (fig 3.40) and spheres (more prevalent) that are commonly arranged into either clusters or chains (fig 3.41). Given the relative prevalence of these two residue types, the low electron density of both residual materials and the fact that the medium in which nanorods are suspended within and cast from for imaging is ethanol, it is hypothesised that the globular balls correspond to residual polycarbonate (insoluble in ethanol) and the smears correspond to the residual wetting agent poly(vinyl pyrrolidone) (soluble in ethanol).

In any case, such a significant volume of residual material is undesirable, as it could possibly influence the block copolymer microphase separation process and end morphology. In addition, the fact that the nanorods become coated with the residue means that the spatial location of the nanorods will be controlled by interactions between the surface residue and block copolymer, precluding any control due to the surface chemistry of the metal nanorods. Clearly, improved methods of nanorod collection needed to be developed to overcome this issue.

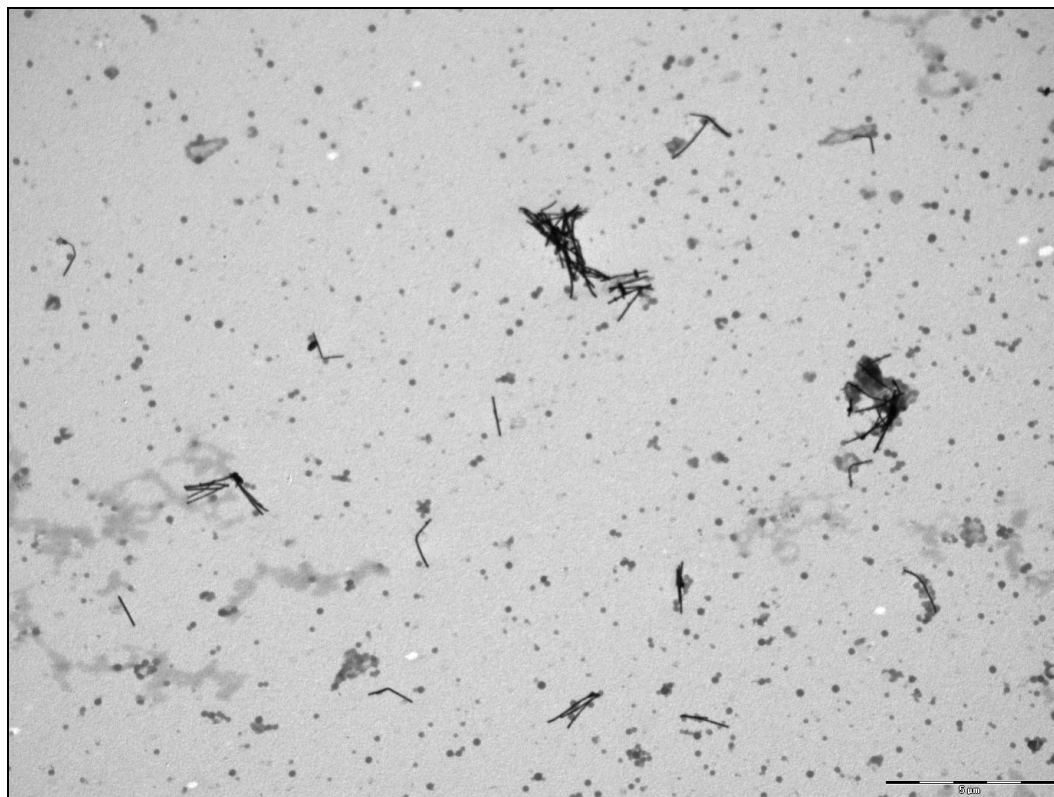


Fig 3.39: TEM image of nanorods collected using the standard literature method of multiple centrifugation and re-suspension steps.

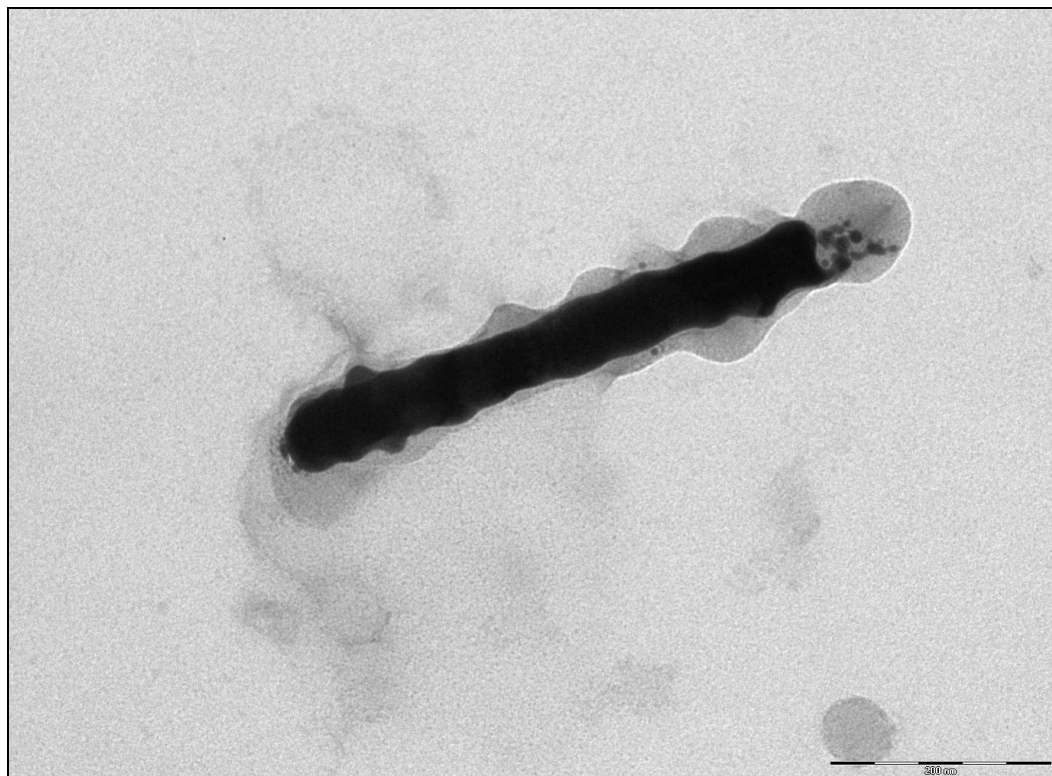


Fig 3.40: TEM image of a nanorod coated in a low electron density residue.

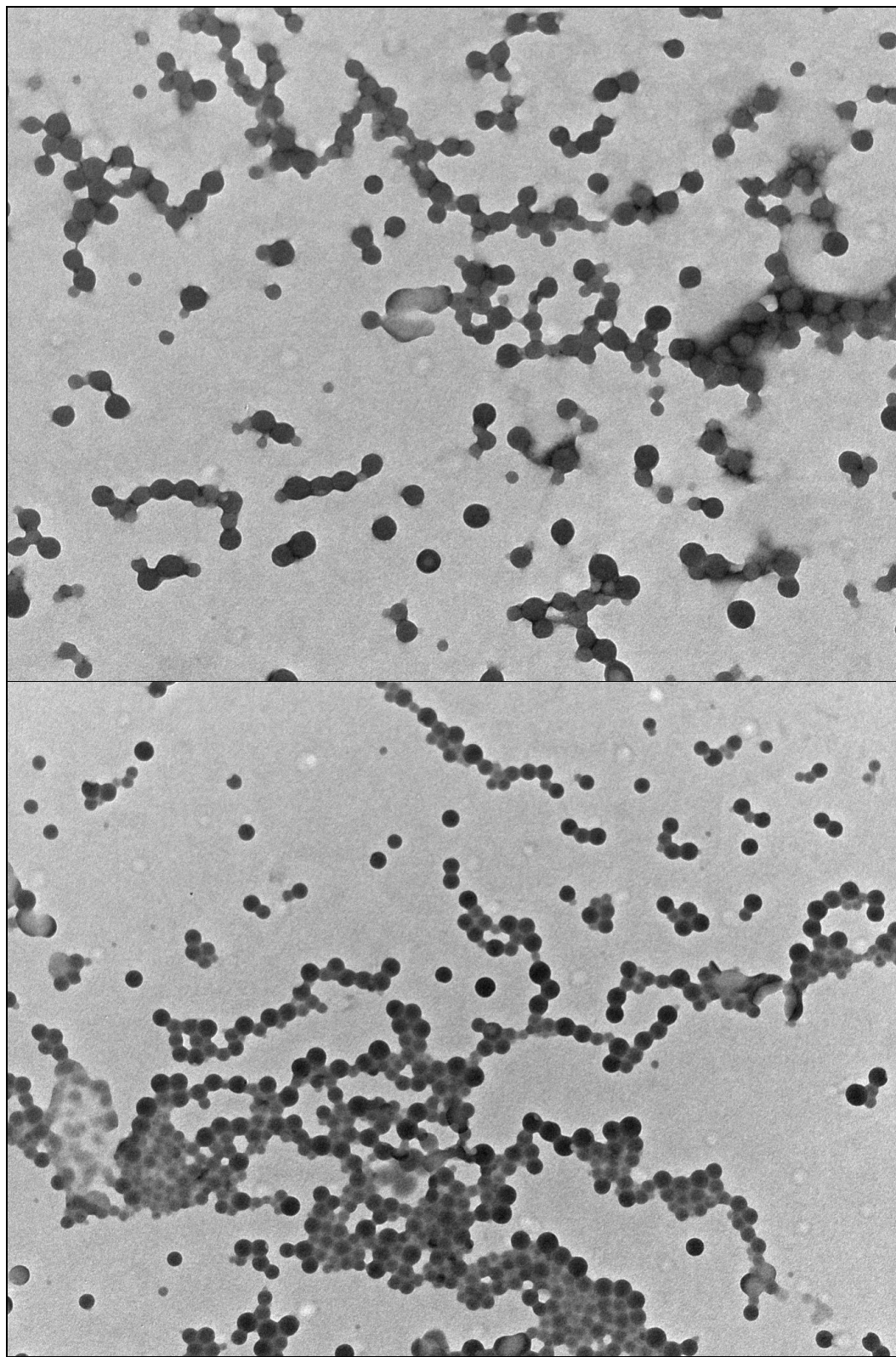


Fig 3.41: TEM images of low electron density spheres present in nanorod samples treated using the standard literature method.

One possible reason for the presence of the residual polymer in these samples is that the shaking / mild sonication used to break up the sedimented nanorod pellets is insufficient to fully separate the polymer from the nanorods. Use of a more thorough rinsing procedure (involving extensive sonication during the re-suspension steps to help separate the sedimented polymer and nanorods) indicates that this is the case, showing that the residual polymer is almost completely removed (fig 3.42 – 3.43).

However, it was also observed that as the residue is removed in successive centrifugation/re-suspension cycles, the nanorods took progressively longer to sediment sufficiently to allow for removal of the supernatant (up to several hours). Clearly the residue binds the nanorods together into larger aggregates which then sediment more readily. The removal of this residue now prevents these aggregates from forming and thus increases the time taken for the nanorods to sediment. Given the number of centrifuge/suspension cycles required to clean the nanorods, the long sedimentation time required to collect the cleaner nanorods, and the fact that sedimentation times are predicted to be longer for the substantially shorter nanorods corresponding to the dimensions desired for use in block copolymer directed templating studies [52], faster methods of nanorod collection are desired.

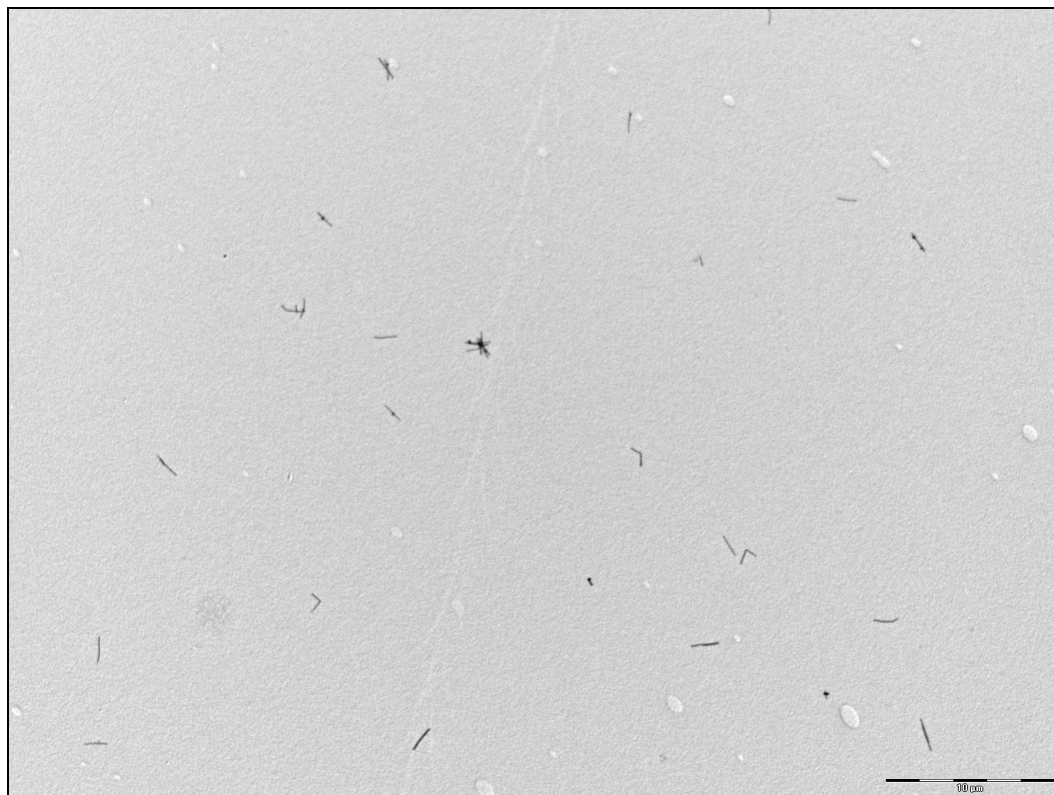


Fig 3.42: TEM image showing the absence of residual polymer when the nanorods are treated with extensive sonication during the re-suspension stage of nanorod collection.

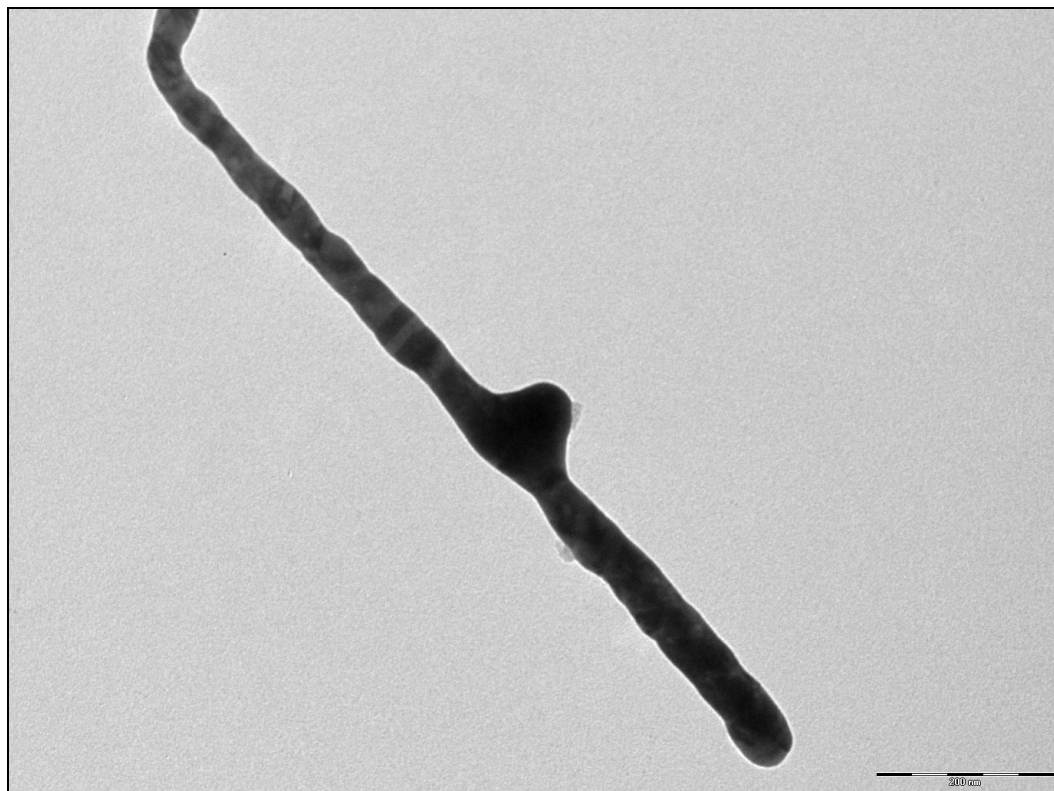


Fig 3.43: TEM image showing the near complete absence of residual polymer adhering to nanorods that are treated with extensive sonication during the re-suspension stage of nanorod collection.

One approach to this problem is to simply increase the sedimentation rate of the nanoparticles. Simply applying a higher centrifugal force on the nanorods should facilitate their more rapid sedimentation. However, a rather large increase in the centrifugal force is required, as forces opposing the sedimentation (buoyancy and viscous drag) are also higher under these conditions, and resist the motion of the nanoparticles. [52] Furthermore, such high centrifugal forces have been known to cause bending and even breakage at the inter-metallic junction between segments of segmented nanorods. [10, 53]

An alternative option is to use a strong magnetic field to sediment the nanorods, as they contain a magnetisable nickel segment. [54] However, unlike the case of much larger nanorods, no visible sedimentation of the nanoparticles (suspended in ethanol) was observed to occur after periods of up to several hours when

nanorod samples comprised of nickel (~ 400nm long) were placed into the magnetic field of a rare earth magnet.

An further alternative involves the removal of the residue in fewer steps, which may be accomplished by chemically digesting the residue using an agent that does not attack the nanorods. Assuming that this residue is indeed polymer, one possible candidate for the removal of the majority residue (polycarbonate) is a strong base, which hydrolyses the carbonate ester linkage of polycarbonate. Aqueous ammonia solution is, in particular, a good candidate for polycarbonate degradation, and would result in the formation of bisphenol A and ammonium carbonate (fig 3.44). [55-56]

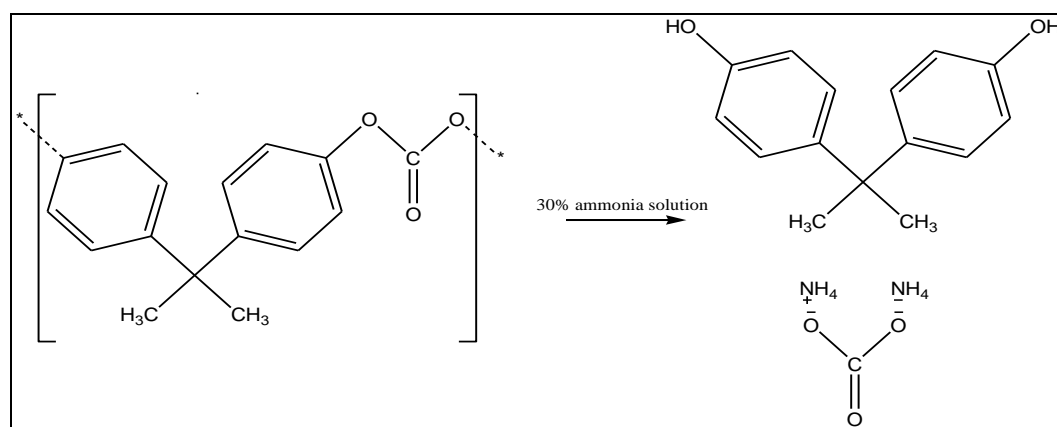


Fig 3.44: diagram showing the chemical attack of polycarbonate by base hydrolysis of the carbonate group.

The use of this method to remove the polycarbonate was tested by treating a membrane containing nickel nanorods (nickel being examined to see if the nanorods remain intact after chemical treatment as potentially they could be attacked chemically in such solutions, whereas gold has been used in such solutions without being etched [57]) with 30% (v/v) ammonia solution for ½ hour (with intermittent sonication to help break up the bulk polymer), and then collecting by centrifugation overnight at a relative centrifugal force of ~1000g. As shown in fig 3.45, this result's in intact nanorod samples where virtually no globular residue is present, suggesting that this residue is indeed polycarbonate.

The smeared residue material that remains after this treatment (fig 3.45 and 3.46) is more evidence that this residue is something other than polycarbonate.

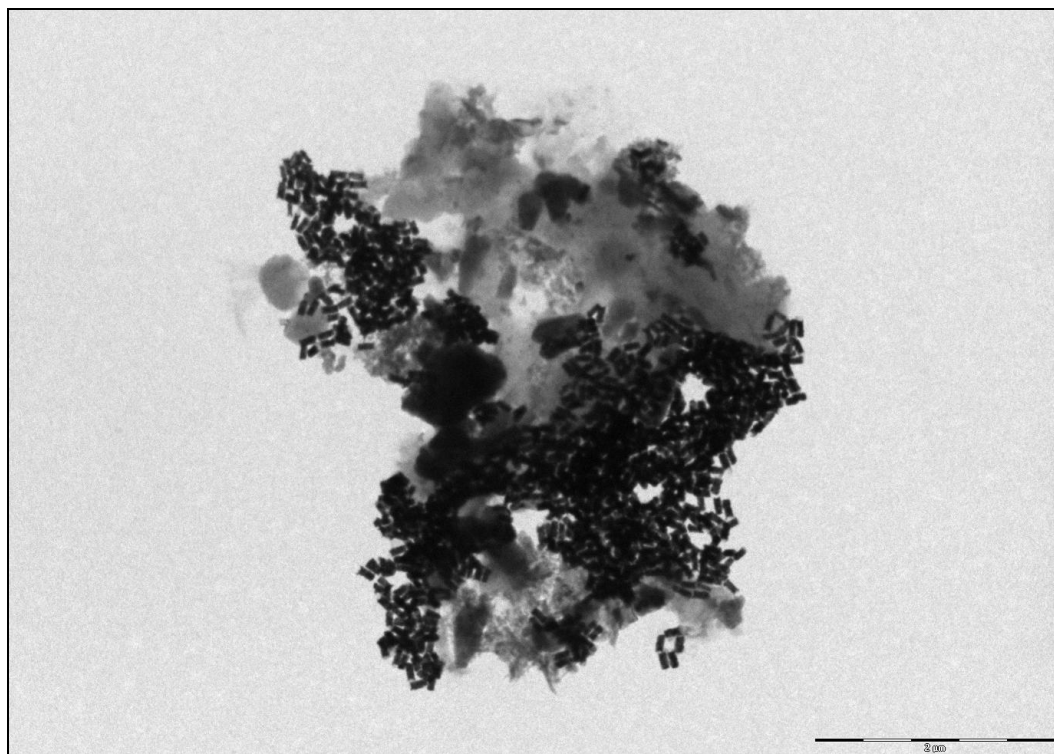


Fig 3.45: TEM image of nanorods collected after treatment with 30% ammonia solution.

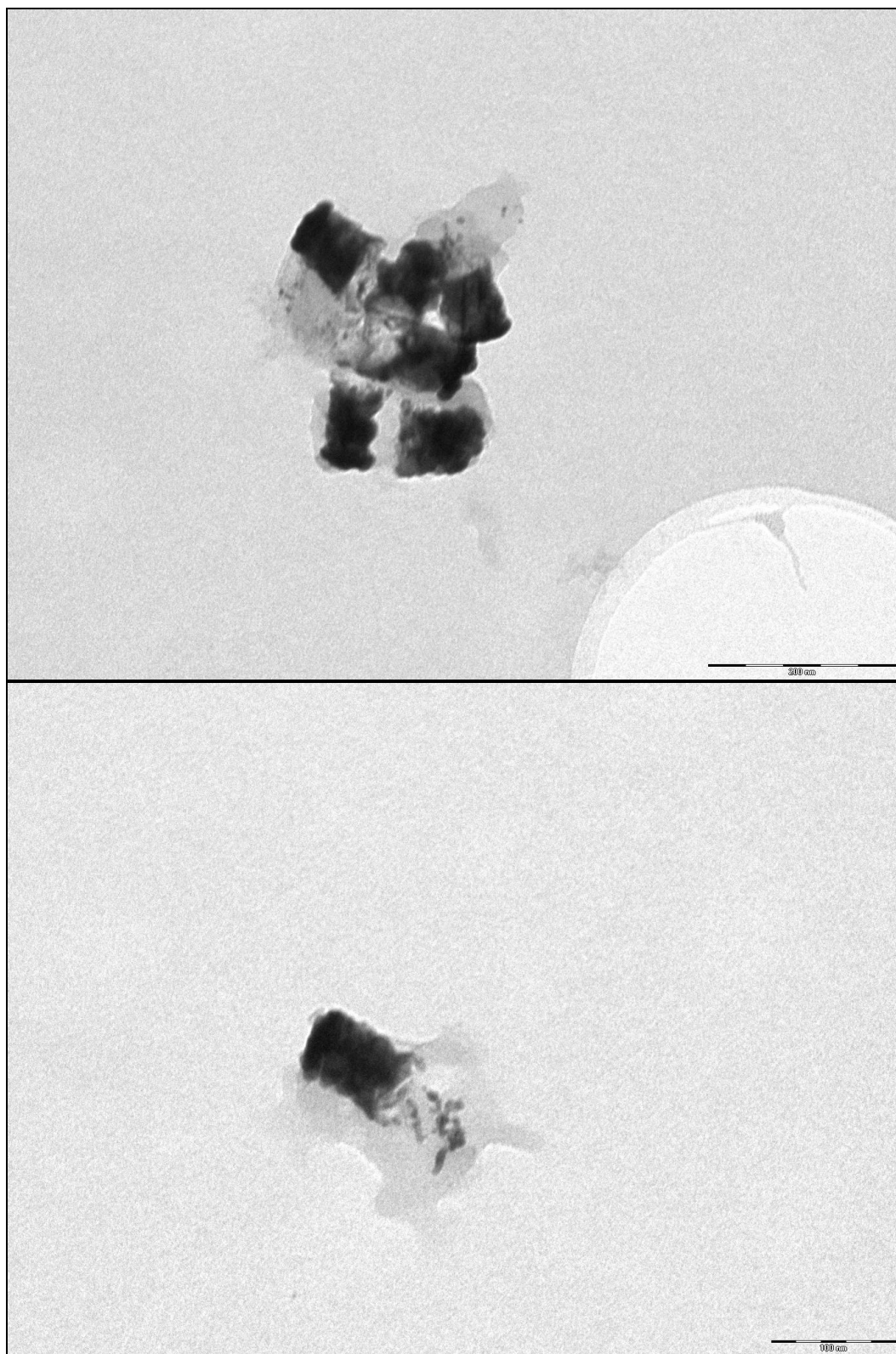


Fig 3.46: TEM images of nanorods collected after treatment with 30% ammonia solution, exhibiting the presence of smears of residue material.

Supposing that the smeared residue material is poly(vinyl pyrrolidone) (noted for its presence on these polycarbonate membranes, its hydrophilic nature and its resistance to ammonia solution), this residue may be removed by oxidative chemical attack by hydrogen peroxide. [58] Such attack would yield 2-(2-oxopyrrolidin-1-yl)acetaldehyde, which would in turn be converted to 2-(2-oxopyrrolidin-1-yl)acetic acid due to oxidation by the hydrogen peroxide (fig 3.47).

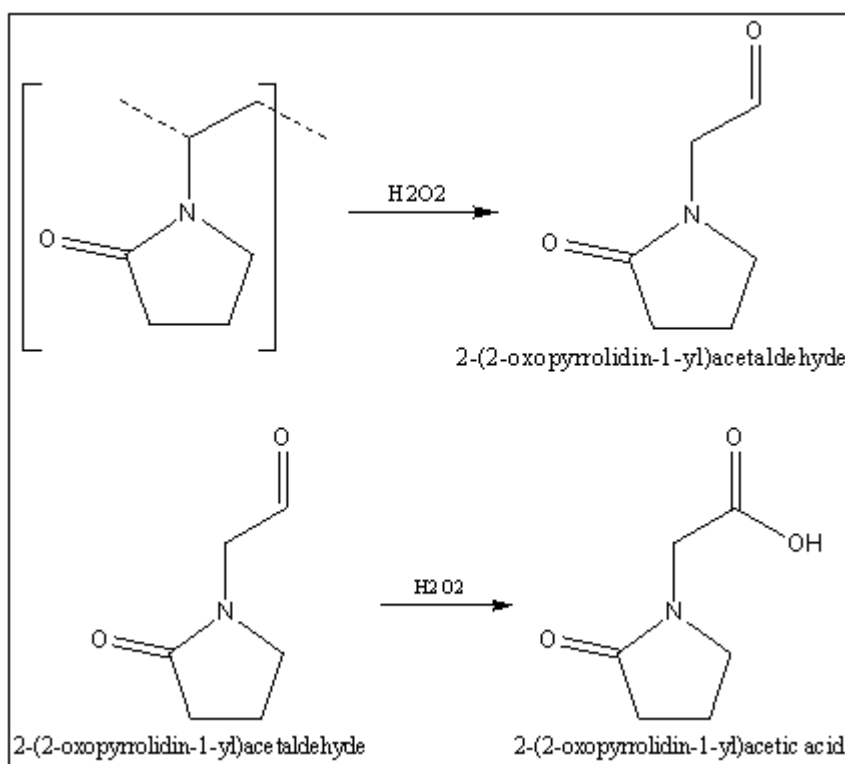


Fig 3.47: diagram depicting the chemical attack of poly(vinyl pyrrolidone) by hydrogen peroxide.

Treatment of nanorods with 30% (v/v) hydrogen peroxide for 1 hour following the removal of the polycarbonate residues (by 30% ammonia solution) and their collection by centrifugation yields intact nanorods that are essentially free of any visible residue (fig 3.48), affirming that this smeared residue material likely poly(vinyl pyrrolidone).

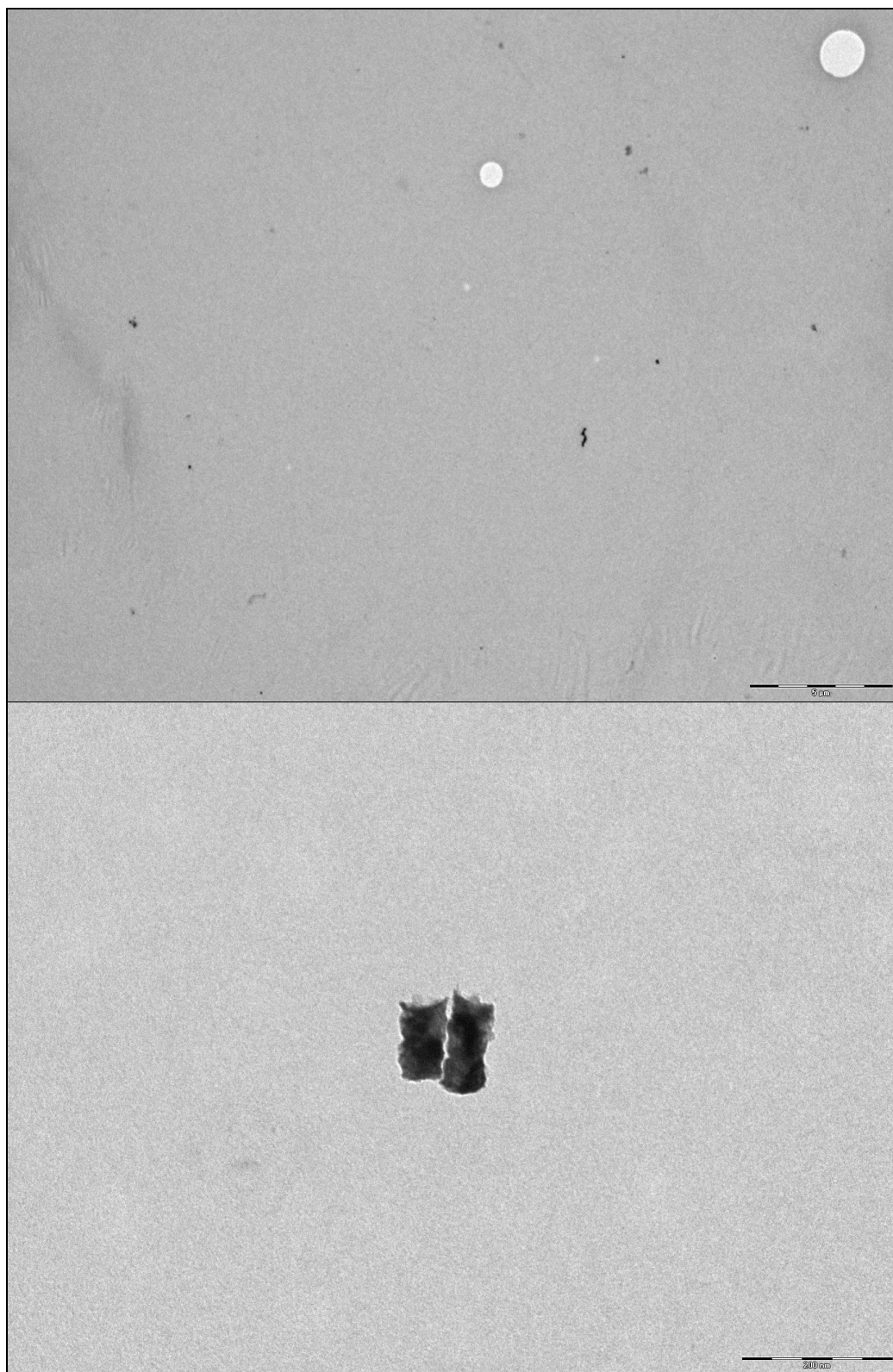


Fig 3.48: TEM images of nanorods treated with 30% ammonia solution followed by 30% hydrogen peroxide solution.

Based on these results, the following nanorod collection procedure was trialed for use in subsequent work:

Nanorods embedded in the polymer membrane were placed into a 10ml polyethylene centrifuge tube, to which was added 3ml of a 30% ammonia solution. After 1 hour of standing (with intermittent sonication) 3ml of 30% hydrogen peroxide solution was then added, upon which the sample was left to stand for at least 1 hour. The nanorods were collected by centrifugation, and the nanorod pellets rinsed with ethanol.

This particular procedure was devised as it: (a) allows for the most rapid collection of the nanoparticles (only one centrifugation is required), (b) the presence of ammonia during from the decomposition of the poly(vinyl pyrrolidone) converts the resulting carboxylic acids into amides, thereby preventing their binding to the surface of the nickel nanorods (as this may inhibit further functionalisation of the nanorods) (fig 3.49) and (c) the presence of ammonia and trace amounts of metal ions catalyses the decomposition of hydrogen peroxide [59-60], which results in more rapid decomposition of the poly(vinyl pyrrolidone). [58]

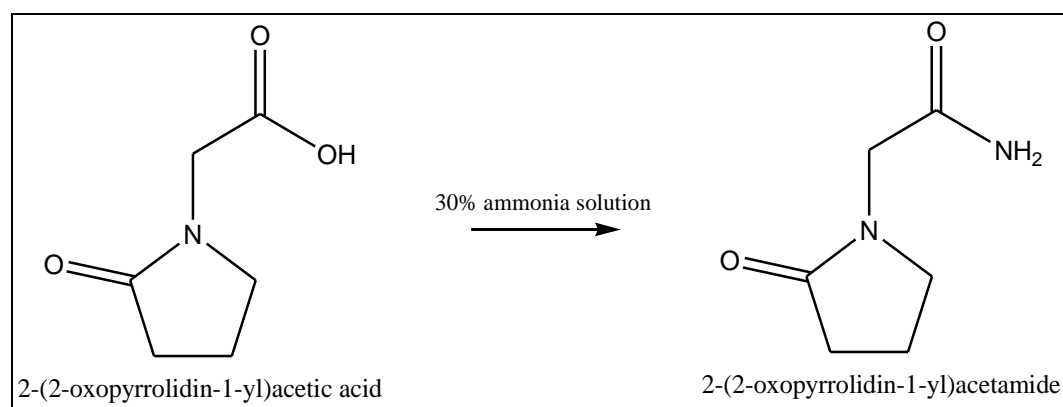


Fig 3.49: diagram depicting the conversion of carboxylic acid by products of poly(vinyl pyrrolidone) into corresponding amides by ammonia.

The volumes of ammonia and hydrogen peroxide solution used in this procedure were calculated so that a large excess of each is present compared to the amount of polymer present, to ensure the decomposition of the polymers and conversion of all the resulting carboxylic acids into ammonium salts:

In the case of the polycarbonate decomposition, if it is assumed that the entire mass of the membrane (30g) is polycarbonate, there is $1.181 \cdot 10^{-4}$ mol of polycarbonate monomer units (based on a molar mass of 254g/mol for bisphenol A carbonate repeat unit) and therefore approximately the same number of ester linkages to be degraded by hydrolysis. 3ml of 30% ammonia solution corresponds to $0.9\text{ml} \cdot 0.6819\text{g/ml} = 0.6137\text{g}$ of ammonia or $3.6 \cdot 10^{-2}$ mol of ammonia, so clearly there is a large excess of ammonia. In the case of Poly(vinyl pyrrolidone) decomposition, if it assumed that the entire mass of the membrane is due to this polymer (a gross exaggeration), then there is $3.125 \cdot 10^{-4}$ mol of poly(vinyl pyrrolidone) monomer units (based on a molar mass of 96g/mol for vinyl pyrrolidone) and therefore approximately the same number of linkages to be attacked. This is significantly less than the number of moles of hydrogen peroxide present in 3 ml of 30% solution ($0.9\text{ml} \cdot 1.463\text{g/ml} = 1.3167\text{g}$ which is equivalent to $3.87 \cdot 10^{-2}$ moles). Furthermore, such decomposition will also yield $3.125 \cdot 10^{-4}$ mol of carboxylic acid by-products, which is much less than the amount of ammonia present in the solution.

TEM images of nanorods treated using this procedure are shown in figure 3.50. As can be seen, virtually the entire sample is polymer free. It is noted that the supernatant in the centrifuge tube is pale yellow after decomposition of the polymer following addition of the H_2O_2 . This is ascribed to the formation of the ammonium carboxylate salts. Note that the collection of the nanorods under these conditions is time consuming in itself (~ 24 hours of centrifugation required to form a stable pellet), but is faster and more effective than the other trialed methods.

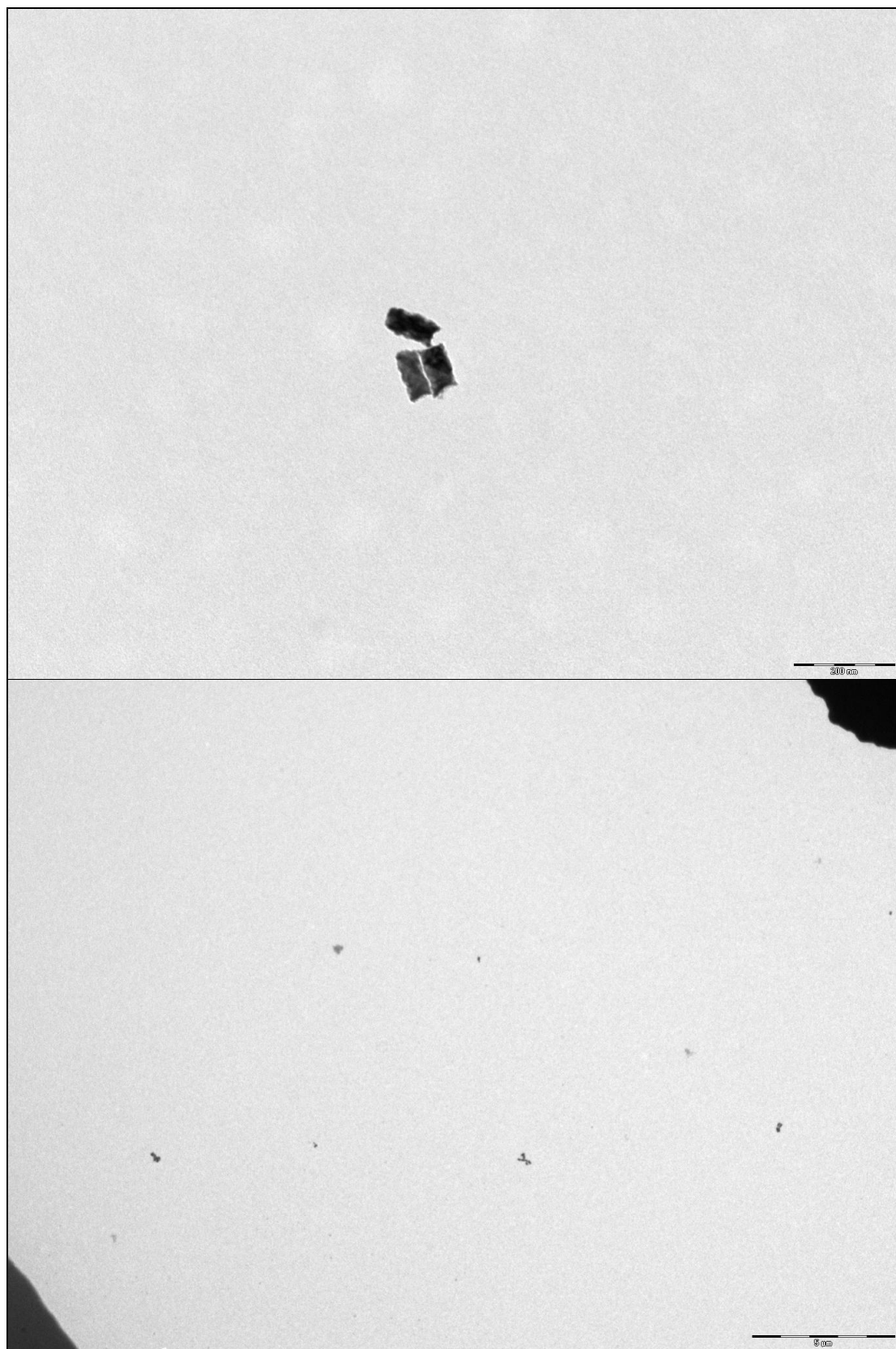


Fig 3.50: TEM images of nanorods treated with ammonia solution and hydrogen peroxide.

3.4. Conclusions

In conclusion, it was found that use of typical literature procedures for the template synthesis of metal nanorods with dimensions suitable for use in template assisted alignment with block copolymers result in nanorods that are compositionally impure, and have a wide range of lengths. Based on the analysis of these results, methods were developed that allowed for significant improvements in both the nanorod segment composition and length distribution. It was found that nanorod composition may be improved by avoiding co-deposition of the intended metal with residual metal species from previous segment formations, through carefully selecting the order of metal deposition and by sonicating the membranes during rinsing between segment depositions to facilitate the removal of the residual metal species from the narrow pores. Nanorods with much more well defined lengths were formed by accounting for variations in mass transport into the different pores of the membrane; achieved by eliminating the effects of an inhomogeneous electric field over the cathode and through a combination of enhanced mass transport into the pores by sonication as well as reducing in the rate of reduction of the metal species.

It was also found that the standard method for collecting these nanorods from the synthesis template is unsuitable for the small nanorods targeted in this work, as it is a very time consuming process, owing to the long sedimentation times required for such small nanoparticles and the necessary multiple centrifugation steps. An improved procedure was developed that involves removal of the polymer template by chemical means, yielding clean nanorods that may be collected much more rapidly, as only a single centrifugation step is required for collection.

3.5. References

1. Lilly, M.P., Wootters, A. H., Hallock, R. B. *Physical Review, B*, 2002. **65**: p. 104503.
2. Schonenberger, C., van der Zande, B. M. I., Fokkink, L. G. J., Henny, M., Schmid, C., Kruger, M., Bachtol, A., Huber, R., Birk, H., Stauffer, U. *Journal of Physical Chemistry, B*, 1997. **101**: p. 5497.
3. Tian, M., Wang, J., Kurtz, J., Mallouk, T. E., Chan, M. H. W. *Nano Letters*, 2003. **3**(7): p. 919.
4. Apel, P.Y., Blonskaya, I. V., Dmitriev, S. N., Orelovitch, O. L., Sartowska, B. *Journal of Membrane Science*, 2006. **282**: p. 393.
5. Sando, G.M., Berry, A. D., Campbell, P. M., Baronavski, A. P., Owrutsky, J. C. *Plasmonics*, 2007. **2**: p. 23.
6. Mock, J.J., Oldenburg, S. J., Smith, D. R., Schultz, D. A., Schultz, S. *Nano Letters*, 2002. **2**(5): p. 465.
7. Pena, D.J., Mbindyo, J. K. N., Carado, A. J., Mallouk, T. E., Keating, C. D., Razavi, B., Mayer, T. S. *Journal of Physical Chemistry, B*, 2002. **106**: p. 7458.
8. Martin, B.R., Dermody, D. J., Reiss, B. D., Fang, M., Lyon, A. L., Natan, M. J., Mallouk, T. E. *Advanced Materials*, 1999. **11**(12): p. 1021.
9. Kline, T.R., Paxton, W. F., Mallouk, T. E., Sen, A. *Angewandte Chemie Internation Edition in English*, 2005. **44**: p. 744.
10. Bauer, L.A., Reich, D. H., Meyer, G. J. *Langmuir*, 2003. **19**: p. 7043.
11. Blair, A. *Metal Finishing*, 2001. **99**(1).
12. Morrissey, R.J. (2008) *Gold and Silver Plating Basics*.
13. Burling, S., Hemsley, S., Hu, J. (2007) *Silver Keeps Pace*.
14. Abdul-Lettif, A.M. *Surface and Interface Analysis*, 2003. **35**(5).
15. Xue, S., Li, M., Wang, Y., Xu, X. *Thin Solid Films*, 2009. **517**(20): p. 5922.
16. Xue, S.H., Wang, Z. D. *Materials Science and Engineering, B*, 2006. **135**(1): p. 74.

17. Sando, G.M., Berry, A. D., Owrutsky, J. C. *Journal of Chemical Physics*, 2007. **127**: p. 074705.
18. Nelson, N.J., *Nickel Etching Process and Solution*, USPTO, Editor. 1985, Psi, Star (Hayward, CA): USA.
19. Natan, M.J., Penn, S. G., Freeman, R. G., Chakarova, G., Doering, W. E., Walton, I. D., *Surface Enhanced Spectrometry-Active Composite Nanoparticles*, USPTO, Editor. 2006.
20. Whitney, T.M., Jiang, J. S., Searson, P. C., Chien, C. L. *Science*, 1993. **261**: p. 1316.
21. Salem, A.K., Searson, P. C., Leong, K. W. *Nature Materials*, 2003. **2**: p. 668.
22. Tierney, M.J., Martin, C. R. *The Journal of Physical Chemistry*, 1989. **93**(8).
23. Gu, Z., Ye, H., Smirnova, D., Small, D., Gracias, D. H. *Small*, 2006. **2**: p. 225.
24. Siooss, J.A., Stoermer, R. L., Sha, M. Y., Keating, C. D. *Langmuir*, 2007. **23**(22): p. 11334.
25. Mirkovic, T., Foo, M. L., Arsenault, A. C., Fournier-Bidoz, S., Zacharia, N. A., Ozin, G. A. *Nature Nanotechnology*, 2007. **2**(9): p. 565.
26. Foss, C.A., Tierney, M. J., Martin, C. R. *Journal of Physical Chemistry*, 1992. **96**: p. 9001.
27. Kumar, A., Kumar, R., Kumar, S., Chakarvarti, S. K. *Current Science*, 2004. **87**(5): p. 642.
28. Pandey, R.K., Sahu, S. N., Chandra, S., *Handbook of Semiconductor Electrodeposition*, ed. S.N. Sahu, Chandra, S. Vol. 5. 1996: CRC Press.
29. Wang, H.-W., et al. *Nanotechnology*, 2006. **17**: p. 2689.
30. *Technical data sheet: Techni-Gold 434*, Technic Inc.
31. Ertan, A., Tewari, S.N., Talu, O. *Journal of Experimental Nanoscience*, 2008. **3**(4): p. 287.
32. Schriver, D.F., Atkins, P.W., *Inorganic Chemistry*. 3rd ed. 1999, Oxford: Oxford University Press.

33. Ji, C., Searson, P.C. Applied Physics Letters, 2002. **4437**: p. 81.
34. Burdick, J., et al. Nanotechnology, 2009. **20**: p. 065306.
35. Yoo, S.H., Park, S. Advanced Materials, 2007. **19**: p. 1612.
36. Liu, Z., Searson, P.C. Journal of Physical Chemistry B, 2006. **110**: p. 4318.
37. Ji, C., et al. Journal of the Electrochemical Society, 2003. **150**(8): p. C523.
38. Ji, C.X., Searson, P.C. Journal of Physical Chemistry B, 2003. **107**: p. 4494.
39. Liu, L., et al. Nanotechnology, 2008. **19**: p. 335604.
40. Dietterle, M., Jordan, M., Strube, G., *Electrolyte and Method for Depositing Tin-Silver Alloy Layers*, USPTO, Editor. 2006, Dr. -Ing. Max Schlotter GmbH & Co. KG (Geislingen/Steige, DE).
41. Myung, N., Sumodjo, P.T.A., Nobe, K. in *Proceedings of the 3rd Symposium on Electrochemically Deposited Thin Films*. 1997: The Electrochemical Society.
42. Bulbarello, A., et al. Small, 2008. **4**(5): p. 597.
43. Van Der Zande, B.M.I., et al. Langmuir, 2000. **16**: p. 451.
44. Ramesh, T.N., Kamath, P.V. Journal of Power Sources, 2006. **156**(2): p. 655.
45. Kuo, T.-C., Sloan, L. A., Sweedler, J. V., Bohn, P. W. Langmuir, 2001. **17**: p. 6298.
46. Leopold, S., et al. Electrochimica Acta, 2002. **47**: p. 4393.
47. Riveros, G., et al. Nanotechnology, 2006. **17**: p. 561.
48. Molaes, M.E.T., Buschmann, V., Dobrev, D., Neumann, R., Scholz, R., Schubert, I. U., Vetter, J. Advanced Materials, 2001. **13**: p. 62.
49. Puipe, J.C., Ibl, N. Journal of Applied Electrochemistry, 1980. **10**(6): p. 775.
50. Dolati, A., Ghorbani, M., Ahmadi, M.R. Journal of Electroanalytical Chemistry, 2005. **577**(1): p. 1.
51. Bozzini, B., et al. Journal of Materials Science, 2002. **37**(18): p. 3903.

52. Sharma, V., Park, K., Srinivasarao, M. Proceedings of the National Academy of Sciences, 2009. **106**(13): p. 4981.
53. Reiss, B.D., et al. Journal of Electroanalytical Chemistry, 2002. **522**: p. 95.
54. Lee, K.-B., Park, S., Mirkin, C.A. Angewandte Chemie, 2004. **116**(23): p. 3110.
55. Brunelle, D.J., *Polycarbonates*, in *Encyclopedia of Polymer Science and Technology*. 2006, John Wiley and Sons, Inc.
56. Brydson, J.A., *Plastics Materials*. 7th ed. 1999: Butterworth-Heinemann.
57. Arikawa, S., Murakami, H., *Method of manufacturing semiconductor device terminal having a gold bump electrode.*, USPTO, Editor. 1994, Seiko Epson Corporation: USA.
58. Panarin, E.F., Gavrilova, I.I. Russian Journal of Applied Chemistry, 1997. **70**(12): p. 1993.
59. *Stabilisation of aqueous solutions containing hydrogen peroxide, hydrofluoric acid and metal ions*, USPTO, Editor. 1985, Atochem: France.
60. van der Meerakker, J.E.A.M., van der Straaten, M.H.M. Journal of the Electrochemical Society, 1990. **137**(4): p. 1239.